


Two-particle states in one-dimensional coupled Bose-Hubbard modelsYabo Li,^{1,2} Dominik Schneble² , and Tzu-Chieh Wei^{1,2}¹*C. N. Yang Institute for Theoretical Physics, State University of New York at Stony Brook, Stony Brook, New York 11794-3840, USA*²*Department of Physics and Astronomy, State University of New York at Stony Brook, Stony Brook, New York 11794-3800, USA*

(Received 13 January 2022; accepted 9 May 2022; published 27 May 2022)

We study dynamically coupled one-dimensional Bose-Hubbard models and solve for the wave functions and energies of two-particle eigenstates. Even though the wave functions do not directly follow the form of a Bethe ansatz, we describe an intuitive construction to express them as combinations of Choy-Haldane states for models with intra- and interspecies interactions. We find that the two-particle spectrum of the system with generic interactions comprises in general four different continua and three doublon dispersions. The existence of doublons depends on the coupling strength Ω between two species of bosons, and their energies vary with Ω and interaction strengths. We give details on one specific limit, i.e., with infinite interaction, and derive the spectrum for all types of two-particle states and their spatial and entanglement properties. We demonstrate the difference in time evolution under different coupling strengths and examine the relation between the long-time behavior of the system and the doublon dispersion. These dynamics can in principle be observed in cold atoms and might also be simulated by digital quantum computers.

DOI: [10.1103/PhysRevA.105.053310](https://doi.org/10.1103/PhysRevA.105.053310)**I. INTRODUCTION**

The Bose-Hubbard model (BHM), known as one of the simplest models that captures the essence of the superfluid–Mott-insulator transition [1], has given rise to a plethora of studies with cold bosonic atoms in optical lattices [2–5] in which the ratio between hopping and on-site interaction is widely tunable. Extensions to multicomponent BHMs enable studies of polaron physics [6,7] and quantum magnetism [8–11], and by adding a dynamical coupling between the components it is furthermore possible to implement BHMs that mimic radiative effects [12–15] in waveguide QED [14,16–21], featuring fractional decay, bound states [22,23], and polaritons [15,24,25]. This also provides a connection to photon-based many-body physics [24,26,27] in the microwave domain [28–32].

The recent implementation of matter-wave polaritons [15,25] motivates a deeper understanding of the coupled BHM beyond a single excitation. There have already been some theoretical works on two-particle and multiparticle waveguide QED and qubit-photon coupled systems using variational and perturbative methods [16,24]. In this paper, rather than attempting to solve the full many-body problem, we give an analytical description of the states with one and two excitations in a one-dimensional coupled Bose-Hubbard model, including the spectrum under different parameters, as well as properties of the states in the continua and of the bound states [14,24,33]. The bound states are the so-called doublon states [34,35], whose wave function is localized in space. In the single-species Bose-Hubbard model, doublon states [34,35] exist outside the two-particle scattering continuum. When the interaction strength approaches infinity, i.e., $U \rightarrow \infty$, the doublon states form repulsively bound atom pairs that have a well-defined total momentum.

In this work we consider the coupled Bose-Hubbard model and provide the complete solution for its two-particle eigenstates. When the intraspecies $U \rightarrow \infty$ and the Rabi coupling Ω is not small (on the scale of the hopping), we show below that the doublon states correspond to two particles residing on the same site for different species, but on adjacent sites for the same species, which we will refer to as the adjacency feature. When we specify the initial state, by exciting specific empty sites and letting them evolve, we observe in numerical simulations that the wave function decays incompletely, which is the hallmark of the non-Markovian regime [23]. When two copies of the same Bose-Hubbard model are coupled together, one of the doublons naturally lies inside a continuum (different types of states will be explained in detail in Sec. VII). This makes it a bound state in the continuum [36,37] that is robust in a compact (finite-size) system. In some other Hubbard models, there are also bound states that can move into and out of the continuum continuously [38–40]. Bound states in the continuum provide potential applications for quantum memory and some other quantum information processing [41–43].

The Bethe ansatz has been a powerful method to infer the exact wave functions of several systems in one dimension, including, e.g., spin chains, the Fermi Hubbard model, and the Kondo problem [44]. In the Bose-Hubbard model, the exact wave functions of many-body states cannot be inferred from the Bethe ansatz. However, when the occupation number per site is smaller than 3, this model is solvable. In fact, in several Bose-Hubbard-like models, the two-particle wave functions can be solved. For example, in Refs. [45–47], the two-particle states were obtained by solving corresponding Schrödinger equations in the infinite system; in Refs. [38,48], the Bethe ansatz was explicitly used. As explained in detail below, in the coupled Bose-Hubbard model, two-particle states can

always be written by a form modified from Bethe ansatz (in the form of a superposition of Choy-Haldane states [49–52]) and solutions to any finite periodic system can be obtained. Viewed from a different perspective, these few-body states in Bose-Hubbard-like models correspond to one-particle states in higher-dimensional systems under synthetic dimension mapping [53].

Our analysis shows that the two-particle spectrum of the system comprises in general four different continua and three doublon dispersions with generic interactions. Their energies vary with interaction strengths. We give details on one specific limit, i.e., with infinite interaction, and analyze the spectrum for all types of two-particle states and their spatial and entanglement properties. We also study the dynamics of the quantities for an initial simple state through demonstration of the time evolution. We observe an interesting relation between the large-timescale behavior of the system and the doublon dispersion.

The remaining structure of the present paper is as follows. In Sec. II we review the model considered and in Sec. III we review the solution in the case of single excitations. In Sec. IV we first review two excitations in the single-species Bose-Hubbard case and then in Sec. V we generalize the solution to the coupled Bose-Hubbard models without interspecies interaction. The result with interspecies interaction is presented in Appendix B. In Sec. VI we discuss the general properties of the doublon states. They have exponentially decaying wave functions in the thermodynamic limit. In Sec. VII we show the detailed wave function and spectrum in the coupled Bose-Hubbard model and use the inverse participation ratio to demonstrate different localization properties of doublon and scattering states. We also discuss their entanglement between the two species of bosons. In Sec. VIII we study the time evolution. We find that the existence of doublon states alter the long-term behavior. We summarize in Sec. IX.

II. MODEL

We consider a system of two species of bosons on a lattice with respective hopping strengths J_1 and J_2 and intraspecies interactions U_1 and U_2 and possibly an energy offset Δ . In addition, there is a direct Rabi coupling Ω between the two species. This is effectively described by the coupled Bose-Hubbard model (assuming the periodic boundary condition $N + 1 \equiv 1$ and single-band approximation)

$$H = \Delta \sum_j a_j^\dagger a_j + \frac{U_1}{2} a_j^\dagger a_j^\dagger a_j a_j + \frac{U_2}{2} b_j^\dagger b_j^\dagger b_j b_j - \sum_{\langle i,j \rangle} (J_1 a_i^\dagger a_j + J_2 b_i^\dagger b_j) + \Omega \sum_j (a_j^\dagger b_j + \text{H.c.}), \quad (1)$$

where i and j are the site indices and $\langle i, j \rangle$ indicates the nearest-neighbor pair of sites. One can also regard this as two ladders (or copies) of the BHM, with the interladder hopping being $-\Omega$. After Fourier transforming from the position space to momentum space, the Hamiltonian is manifestly

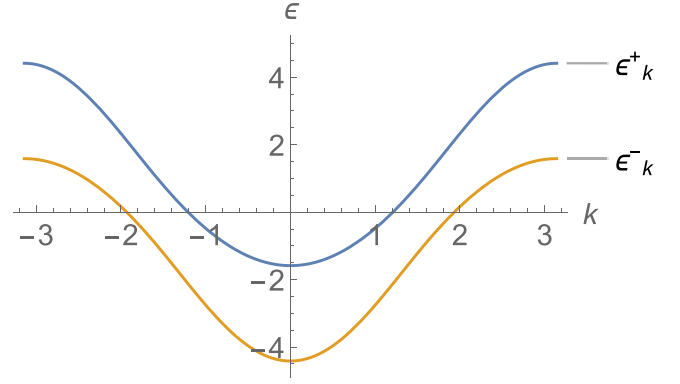


FIG. 1. Dispersion (energy ϵ vs momentum k) of the two one-particle states when $J_1/2 = J_2 = \Omega$ and $\Delta = 0$. The top curve is ϵ_k^+ and the lower curve is ϵ_k^- . The energy ϵ is in units of J_2 .

conserving the total momentum,

$$H = \sum_k (\omega_k a_k^\dagger a_k + \omega'_k b_k^\dagger b_k) + \Omega \sum_k (a_k^\dagger b_k + \text{H.c.}) + \sum_{k,p,q} \frac{U_1}{2N} a_{k-p}^\dagger a_{k+p}^\dagger a_{k-q} a_{k+q} + \frac{U_2}{2N} b_{k-p}^\dagger b_{k+p}^\dagger b_{k-q} b_{k+q}, \quad (2)$$

where $\omega_k = \Delta - 2J_1 \cos k$ and $\omega'_k = -2J_2 \cos k$ arise from tight-binding dispersion relations, with $k = 0, 2\pi/N, \dots, 2\pi(N-1)/N$ labeling the momentum. Since the total particle number operator $\hat{N}_{\text{excitation}} \equiv \sum_k a_k^\dagger a_k + b_k^\dagger b_k$ commutes with H , the Hilbert space can be decomposed into sectors differing by the particle number (also referred to as the excitation number): $N_{\text{excitation}} = 0, 1, 2, \dots$

III. SINGLE EXCITATIONS

We study below eigenstates in the $N_{\text{excitation}} = 1, 2$ subspaces and note that those in the $N_{\text{excitation}} = 2$ subspace can be written in the form of Choy-Haldane states [49], which we review in the next section for a single-species Bose-Hubbard model.

Without loss of generality we write the state of single excitations in the form

$$|\psi\rangle = \sum_k (A_k a_k^\dagger + B_k b_k^\dagger) |0\rangle \quad (3)$$

and plug it into the Schrödinger equation

$$H |\psi\rangle = \epsilon |\psi\rangle \quad (4)$$

to obtain

$$\omega_k A_k + \Omega B_k = \epsilon A_k, \quad (5)$$

$$\Omega A_k + \omega'_k B_k = \epsilon B_k. \quad (6)$$

Then the eigenenergy is the eigenvalue of this 2×2 matrix:

$$\epsilon_k^\pm = [\omega_k + \omega'_k \pm \sqrt{(\omega_k - \omega'_k)^2 + 4\Omega^2}]/2. \quad (7)$$

We show in Fig. 1 an example of the resultant dispersions. When the coupling Ω is large enough, the spectrum splits

into two parts, whose energy does not overlap, and the wave functions are roughly symmetric and antisymmetric between the a and b components, respectively.

Given the solution in momentum space, we could use the Fourier transform to bring the solution back to the position space, such as the components of the wave function, $A_j = \frac{1}{\sqrt{N}} \sum_k A_k e^{ijk}$ and $B_j = \frac{1}{\sqrt{N}} \sum_k B_k e^{ijk}$. We note that when the context is clear, we use the same symbols A and B in both the position and the momentum spaces. While our analysis above assumes the single-band approximation used in the Bose-Hubbard model, the effects of multibands can be taken into account; see, e.g., Ref. [15] for a full analytical description of single excitation. We focus on two-excitation solutions below.

IV. TWO-EXCITATION SOLUTIONS

Having reviewed the single-excitation states, we now turn to two-excitation states. We will first review what was done previously for the single-species Bose-Hubbard model [45,49–52] and then discuss our results for the coupled case in the next section.

Review of the single-species Bose-Hubbard model

We first recall the Hamiltonian in position space

$$H = \Delta \sum_j a_j^\dagger a_j - J \sum_j (a_j^\dagger a_{j+1} + \text{H.c.}) + \frac{U}{2} \sum_j a_j^\dagger a_j^\dagger a_j a_j, \quad (8)$$

which can be equivalently expressed in momentum space

$$H = \sum_k \omega_k a_k^\dagger a_k + \frac{U}{2N} \sum_{k,p,q} a_{k-p}^\dagger a_{k+p}^\dagger a_{k-q} a_{k+q}, \quad (9)$$

where $\omega_k = \Delta - 2J \cos k$. We assume the two-excitation wave function to be of the form

$$|\psi\rangle = \sum_{nm} A_{nm} a_n^\dagger a_m^\dagger |0\rangle = \sum_{pq} A_{pq} a_p^\dagger a_q^\dagger |0\rangle, \quad (10)$$

where n and m are site indices ranging from 0 to $N - 1$, and p and q are momentum variables, ranging from $(2\pi \times 0)/N$ to $2\pi \times (N - 1)/N$. Note that we have abused the notation for the coefficients A in both position and momentum representations, as the context will be clear. In the momentum space, since the total momentum is conserved, we can denote it by P . Then the only nonzero components are those with momentum indices satisfying $p + q = P$. We will thus abbreviate $A_{p,P-p}$ as $A_p^{(P)}$ (or even A_p) for simplicity in the following. Then, similar to the one-excitation case, the Schrödinger equation gives

$$A_p = \frac{U}{N} \frac{A^{(P)}}{\epsilon - \omega_p - \omega_{P-p}}, \quad (11)$$

where $A^{(P)} \equiv \sum_k A_{k,P-k}$ and ϵ is the eigenenergy.

The position wave function $A_{n,m}$ is a symmetric matrix, and we can write the position-space Schrödinger equations as a matrix equation

$$\epsilon A + TA + AT - UD_A = 0, \quad (12)$$

where the hopping matrix $T_{nm} = J(\delta_{n,m-1 \bmod N} + \delta_{n,m+1 \bmod N})$ and D_A is the diagonal part of A , representing double

occupancy of a site. The solutions of this matrix equation are of the Choy-Haldane type [49–52],

$$A_{n,m} = \begin{cases} e^{ikn+iqm} + s_{k,q} e^{iqn+ikm}, & n \leq m \\ A_{m,n}, & n > m, \end{cases} \quad (13)$$

where

$$s_{k,q} \equiv [2J(\sin k - \sin q) - iU]/[2J(\sin k - \sin q) + iU]. \quad (14)$$

One can verify that this is a solution by substituting this form $A_{n,m}$ into the matrix equation (12) above. For the periodic boundary condition, the quasimomentum k (also known as the Bethe parameter) satisfies

$$e^{-ikN} = \frac{2J(\sin k - \sin q) - iU}{2J(\sin k - \sin q) + iU}, \quad (15)$$

and $q = P - k$ from the momentum conservation. Note that from this constraint we know that for a generic $U \neq 0$, the quasimomentum k is not a well-defined momentum on the lattice, i.e., not a physical momentum, with the latter being $\frac{2\pi}{N} \times \text{integer}$. The wave function (11) in space should be related to that (13) in momentum by the Fourier transform: $A_{n,m} = \frac{1}{N} \sum_{p,P} A_p^{(P)} e^{ink+im(P-k)}$.

Equation (15) is referred to as the Bethe equation [44]. Given the parameters J and U and the total momentum P , there are $N - 1$ real solutions in the continuum and one complex solution outside the continuum. The latter, for $U > 0$, is a repulsive bound pair state (attractive for $U < 0$), in which two particles are located at the same sites. The whole two-excitation spectrum for fixed $U/J = 5$ is shown in Fig. 2(a), where one can see the continuum (i.e., a band) and a separate dispersion curve above. To illustrate the dependence of the spectrum as the interaction U changes, in Fig. 2(b) we display the energy at total momentum $P = 0$ horizontally and vary U vertically. This form of the interaction-dependent zero-momentum diagram will be used extensively below.

The state outside the continuum (whose dispersion is represented by the curve above the continuum band) is called a doublon state [34], which is a two-particle bound state (in the relative coordinate). In the case of repulsive interaction, it may seem counterintuitive to have a stable bound state of high energy, but one can understand its existence intuitively as the pair is unable to decay by converting the potential energy into the kinetic energy [35]. In terms of the mathematics, the corresponding quasimomentum of a doublon state is complex, reflecting the nature of bound states, whose expression is $k = \frac{P}{2} + \pi - iK$ if $U > 0$ and $k = \frac{P}{2} - iK$ if $U < 0$, where the imaginary part $K > 0$ is determined by the Bethe equation. When $N \rightarrow \infty$, i.e., in the thermodynamic limit, the left-hand side of the Bethe equation approaches 0. Thus the equation becomes $2J \cos \frac{P}{2} \sinh K = U$. The wave function of the doublon state is thus

$$A_{n,m} = \begin{cases} e^{-K|n-m|} e^{i(P/2+\pi)(n+m)} & \text{when } U > 0 \\ e^{-K|n-m|} e^{i(P/2)(n+m)} & \text{when } U < 0. \end{cases} \quad (16)$$

We can clearly see the bound-state feature of the exponential decay in the relative position of the two particles, i.e., $e^{-K|n-m|}$. We note that an alternative approach to the one described above [49–52] was also given in Refs. [35,45] by solving the scattering problem for two bosons.

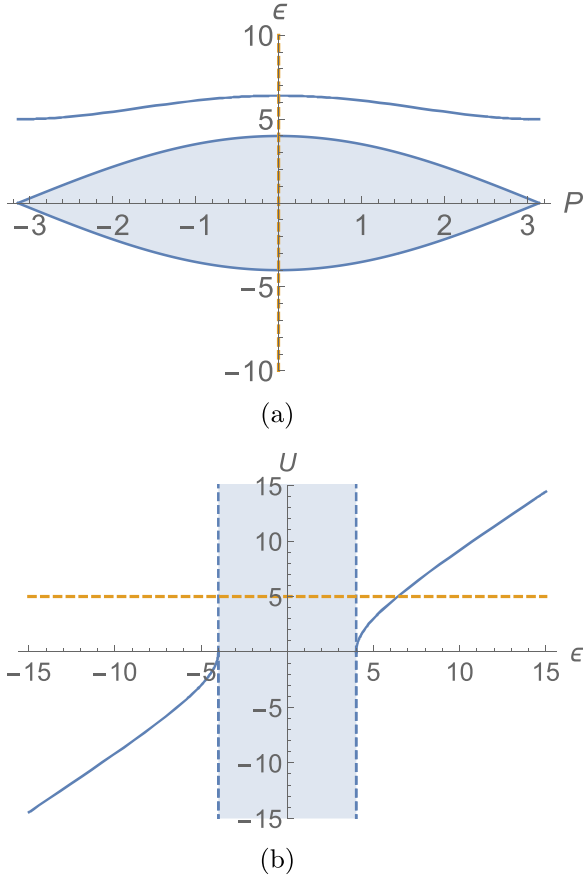


FIG. 2. (a) Dispersion of the continuum band and doublon for $U/J = 5$. The yellow dashed line indicates the spectrum with total momentum $P = 0$, which contains a continuum in the shaded region (formed by the band of two-particle scattering states) and a doublon state outside the continuum. (b) Interaction dependence of the spectrum with total momentum $P = 0$. The yellow dashed line shows the spectrum for a fixed interaction strength $U/J = 5$ and the horizontal section is the same as the corresponding vertical section in Fig. 2(a). We have taken $\Delta = 0$, $J = 1$, and the thermodynamic limit. The energy ϵ is given in units of J .

V. COUPLED BOSE-HUBBARD MODEL WITHOUT INTERSPECIES INTERACTION

Having reviewed the single Bose-Hubbard model case, we now present our main results for the doubly occupied, coupled Bose-Hubbard model, where Ω is the coupling strength. In the momentum space, we can assume that the wave function takes the form

$$|\psi\rangle = \sum_{p,q} (A_{p,q} a_p^\dagger a_q^\dagger + B_{p,q} a_p^\dagger b_q^\dagger + C_{p,q} b_p^\dagger b_q^\dagger) |0\rangle. \quad (17)$$

Then the corresponding Schrödinger equations are

$$\begin{aligned} (\epsilon - \omega_p - \omega_q) A_{p,q} &= \frac{U_1}{N} \sum_{p+q=P} A_{p,q} + \frac{\Omega}{2} (B_{p,q} + B_{q,p}), \\ (\epsilon - \omega_p - \omega'_q) B_{p,q} &= 2\Omega A_{p,q} + 2\Omega C_{p,q}, \\ (\epsilon - \omega'_p - \omega'_q) C_{p,q} &= \frac{U_2}{N} \sum_{p+q=P} C_{p,q} + \frac{\Omega}{2} (B_{p,q} + B_{q,p}). \end{aligned} \quad (18)$$

Since $\sum_{p+q=P} A_{p,q}$ and $\sum_{p+q=P} C_{p,q}$ are constants after fixing the total momentum P , we simply denote them by A and C , respectively. Solving for $A_p \equiv A_{p,P-p}$ and $C_p \equiv C_{p,P-p}$, we arrive at

$$A_p = \frac{1}{(\epsilon - \omega_p - \omega_q - \eta_{pq})(\epsilon - \omega'_p - \omega'_q - \eta_{pq}) - \eta_{pq}^2} \times \left((\epsilon - \omega'_p - \omega'_q - \eta_{pq}) \frac{U_1 A}{N} + \eta_{pq} \frac{U_2 C}{N} \right), \quad (19)$$

$$C_p = \frac{1}{(\epsilon - \omega_p - \omega_q - \eta_{pq})(\epsilon - \omega'_p - \omega'_q - \eta_{pq}) - \eta_{pq}^2} \times \left(\eta_{pq} \frac{U_1 A}{N} + (\epsilon - \omega_p - \omega_q - \eta_{pq}) \frac{U_2 C}{N} \right), \quad (20)$$

where $\eta_{pq} \equiv \Omega^2 \left(\frac{1}{\epsilon - \omega_p - \omega'_q} + \frac{1}{\epsilon - \omega'_p - \omega_q} \right)$ and $q = P - p$. If we further sum over the momentum index p in the above equations, we would have two linear homogeneous equations for A and C . To have a nontrivial wave function, the determinant of the 2×2 matrix should be zero. From this we derive the energy for every given value of the total momentum P . This allows us to solve for the two-excitation spectrum. We leave some of the details to Appendix A. In the following, we only use the momentum-space result, such as in Eqs. (19) and (20), to guide our main approach that generalizes the real-space Choy-Haldane solution from the single-species case, which is in some sense a Bethe ansatz approach.

A. Two-species BHM with coupling Ω

Let us take the simplest case, i.e., $J_1 = J_2 = J$, $\Delta = 0$, and $U_1 = U_2 = U$. Then we have two identical single-body spectra $\omega_p = \omega'_p = -2J \cos p$. The 2×2 coefficient matrix mentioned in the preceding paragraph [see also Eq. (A6) in Appendix A and the discussion therein] has eigenvectors as $A = -C$ and $A = C$. In the former case, $B_{p,q} = 0$, and the equation for $A_{p,q}$ (or $C_{p,q} = -A_{p,q}$) reduces to the Schrödinger equation for the (single-species) Bose-Hubbard model,

$$A_{p,q} = \frac{1}{\epsilon - \omega_p - \omega_q} \frac{UA}{N}, \quad (21)$$

which we have seen in Eq. (11). Therefore, in this case we have just a single Choy-Haldane state and the solution for A is identical.

In the case when $A_{p,q} = C_{p,q}$, $B_{p,q} \neq 0$ and we should not expect the wave function to be just a single Choy-Haldane state. Observing that, when $A = C$, Eq. (19) for A can be rewritten as

$$\begin{aligned} A_p &= \frac{\epsilon - \omega_p - \omega_q}{(\epsilon - \omega_p - \omega_q - \eta_{pq})(\epsilon - \omega_p - \omega_q - \eta_{pq}) - \eta_{pq}^2} \frac{UA}{N} \\ &= \frac{1}{2} \left(\frac{1}{\epsilon - \omega_p - \omega_q - 2\Omega} + \frac{1}{\epsilon - \omega_p - \omega_q + 2\Omega} \right) \frac{UA}{N}. \end{aligned} \quad (22)$$

It is useful to note that the two terms in A_p are of similar form to Eq. (21), i.e., the momentum representation of a Choy-Haldane state, except having an extra constant $\pm 2\Omega$ in the denominator. Since $\pm 2\Omega$ is a constant, we can absorb it separately into ϵ in the respective denominator. Therefore, we expect that in the case when $A_{p,q} = C_{p,q}$, the solution is

a superposition of two Choy-Haldane states, in which ϵ is replaced by $\epsilon + 2\Omega$ and $\epsilon - 2\Omega$, respectively, and we write this symbolically as $|\psi\rangle = |HC_1\rangle + \lambda |HC_2\rangle$, where λ denotes the relative weight to be determined.

From the preceding section, we know that a single Choy-Haldane state is characterized by the scattering factor $s_{k,q}$. One expects the two Choy-Haldane states here to have their own respective (fictitious) interaction strengths, which determines the factor $s_i = [2J(\sin k - \sin q) - i\tilde{U}_i]/[2J(\sin k - \sin q) + i\tilde{U}_i]$. (Notice that we put a tilde on U_i to indicate that it is *not* the physical interaction strength in the Hamiltonian.) However, would the conjectured superposition be a consistent solution as \tilde{U}_i 's are not the physical interaction U ? In other words, can \tilde{U}_i 's be consistently determined from the system's parameters, such as the physical interaction strength U , the total energy ϵ , and the total momentum P ?

It turns out that not only does this superposition trick work, but we also can determine U_i 's in terms of physical parameters. In this and the following examples, we even obtain simple relations between \tilde{U}_i and the physical interaction U .

The way to determine the two fictitious interaction strengths \tilde{U}_1 and \tilde{U}_2 begins as follows. From the energy equation for the two Choy-Haldane states,

$$\epsilon - 2\Omega = \omega_{k_1} + \omega_{P-k_1}, \quad (23)$$

$$\epsilon + 2\Omega = \omega_{k_2} + \omega_{P-k_2}, \quad (24)$$

where k_1 and k_2 are the quasimomenta in $|HC_1\rangle$ and $|HC_2\rangle$, respectively, we have the Bethe equations satisfied by these quasimomenta,

$$e^{-ik_i N} = \frac{2J[\sin k_i - \sin(P - k_i)] - i\tilde{U}_i}{2J[\sin k_i - \sin(P - k_i)] + i\tilde{U}_i} \equiv s_i, \quad (25)$$

for $i = 1, 2$. Furthermore, making use of the Schrödinger equation for $B_{n,m}$, we find that \tilde{U}_i 's are related to U via

$$U = \frac{2\tilde{U}_1\tilde{U}_2}{\tilde{U}_1 + \tilde{U}_2}. \quad (26)$$

From the three equations above, we finally obtain the relation of the energy ϵ to the interaction strength U and the total momentum P .

We now elaborate on the steps to obtain Eq. (26). To do this, we use the Schrödinger equations in the position space, which when $J_1 = J_2$ are

$$\begin{aligned} \epsilon A + TA + AT - UD_A &= \Omega B_s, \\ \epsilon B + TB + BT &= 2\Omega(A + C), \\ \epsilon C + TC + CT - UD_C &= \Omega B_s, \end{aligned} \quad (27)$$

where $B_s \equiv (B + B^T)/2$ is the symmetric part of B and we also define $B_a \equiv (B - B^T)/2$ to be the antisymmetric part of B . Note that the normalization of our wave function is

$$\sum_{n,m} 2|A_{n,m}|^2 + |B_{n,m}|^2 + 2|C_{n,m}|^2 = 1. \quad (28)$$

When $A = C$, the three equations reduce to two:

$$\begin{aligned} \epsilon A + TA + AT - UD_A &= \Omega B_s, \\ \epsilon B + TB + BT &= 4\Omega A. \end{aligned} \quad (29)$$

Let us assume $B_a = 0$ for now (we will return to the scenario $B_a \neq 0$ below); then we have $B_s = B$. Taking A to be a superposition of two Choy-Haldane states with different weights, $A = \psi_1 + \lambda\psi_2$, with these two states ψ_1 and ψ_2 (in matrix form) each satisfying an equation similar to the single-species case in Eq. (12),

$$\begin{aligned} (\epsilon - 2\Omega)\psi_1 + T\psi_1 + \psi_1 T - \tilde{U}_1 D_{\psi_1} &= 0, \\ (\epsilon + 2\Omega)\psi_2 + T\psi_2 + \psi_2 T - \tilde{U}_2 D_{\psi_2} &= 0, \end{aligned} \quad (30)$$

where, for convenience, D_{ψ_1} and D_{ψ_2} are used to denote the diagonal parts of ψ_1 and ψ_2 , respectively. Note that *if*

$$\tilde{U}_1(1 + s_1) + \lambda\tilde{U}_2(1 + s_2) = U(1 + s_1) + \lambda U(1 + s_2), \quad (31)$$

then, according to the first Schrödinger equation, $B = 2(\psi_1 - \lambda\psi_2)$. With this, we can use the other equation to obtain another relation for the parameter λ and the \tilde{U}_i 's:

$$\tilde{U}_1(1 + s_1) - \lambda\tilde{U}_2(1 + s_2) = 0. \quad (32)$$

Solving the above two equations, we obtain the relation $U = 2\tilde{U}_1\tilde{U}_2/(\tilde{U}_1 + \tilde{U}_2)$.

To conclude the above calculations, we have shown that the matrices for the wave function, A and C (as well as B , if nonzero), can be written as combinations of two Choy-Haldane states, each with a fictitious interaction strength \tilde{U}_i . Since the diagonal part of the Choy-Haldane state is $D_{nm} = (1 + s)e^{iPn}\delta_{nm} \propto e^{iPn}\delta_{nm}$, we have recombined the diagonal parts in two Choy-Haldane states as in Eq. (31) to satisfy the Schrödinger equation, in which the diagonal term is proportional to the physical interaction, i.e., UD_A or UD_C . This is a key part in obtaining the wave function as a sum of Choy-Haldane states. We will use this ‘‘recombination’’ technique below for the generic case.

1. Doublons

In the thermodynamic limit ($N \rightarrow \infty$), we concentrate on those states outside the continua, which are called doublons. Their wave functions are Choy-Haldane states with complex quasimomenta: $k = a - iK$, $K > 0$. For these states, we can directly write their energy equations given the total momentum P and interaction strength U . There are three separate regions, obtained by solving Eq. (23)–(26),

$$U = -2 \frac{\sqrt{+}\sqrt{-}}{\sqrt{+} + \sqrt{-}} \quad \text{when } \epsilon < -2\Omega, \quad (33)$$

$$U = 2 \frac{\sqrt{+}\sqrt{-}}{\sqrt{+} - \sqrt{-}} \quad \text{when } -2\Omega < \epsilon < 2\Omega, \quad (34)$$

$$U = 2 \frac{\sqrt{+}\sqrt{-}}{\sqrt{+} + \sqrt{-}} \quad \text{when } \epsilon > 2\Omega. \quad (35)$$

where $\sqrt{\pm} \equiv \sqrt{(\epsilon \pm 2\Omega)^2 - 16J^2 \cos^2 \frac{P}{2}}$. We plot the ϵ - U relation for $P = 0$ in Fig. 3(b).

Note that the doublon in between two continua exists in the continuum shown in Fig. 3(a) (in Sec. VII we refer to it as a type-1 vacuum) as long as U is large enough for any Ω . This means that we have a bound state in the continuum.

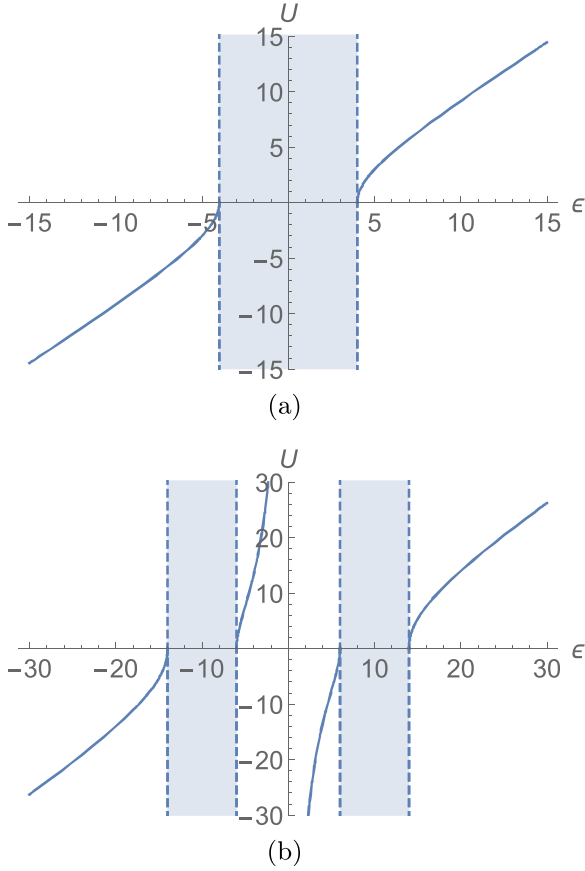


FIG. 3. Spectrum of the coupled Bose-Hubbard model: two-excitation states in the thermodynamic limit, with $\Delta = 0$, $J = 1$, $\Omega = 5$, and $P = 0$ for $U_1 = U_2 = U$. The energy ϵ is in units of J . (a) Spectrum of states satisfying $A_{p,q} = -C_{p,q}$ and $|\psi_1\rangle = |HC_0\rangle$ or satisfying $B = B_a$. (b) Spectrum of states satisfying $A_{p,q} = C_{p,q}$ and $|\psi_2\rangle = |HC_1\rangle + \lambda |HC_2\rangle$.

2. Antisymmetric solutions

Until now we have assumed that the antisymmetric part of B vanishes, i.e., $B_a = 0$. In fact, there is a set of solutions with nonzero B_a . From the Schrödinger equations (27), if $A = C = 0$ and $B = B_a$, the only remaining equation is

$$\epsilon B_a + T B_a + B_a T = 0. \quad (36)$$

The solution of this equation is the antisymmetric Bethe state

$$B_{n,m} = e^{ikn+iqm} - e^{iqn+ikm}, \quad (37)$$

with the Bethe constraint $e^{ikN} = 1$. The corresponding energy is $\epsilon = \omega_k + \omega_q$. In the thermodynamic limit, these solutions form a new continuum in the spectrum, whose energy range coincides with the continuum formed by the case $A = -C$, as in Fig. 3(a). However, the wave functions in the latter are orthogonal to those in the former case as their $B_a = 0$.

B. Case $U_1 \neq U_2$

We can now straightforwardly extend our result to the case when $U_1 \neq U_2$. Notice from Eq. (18) that $A_{p,q}$ and $C_{p,q}$ are

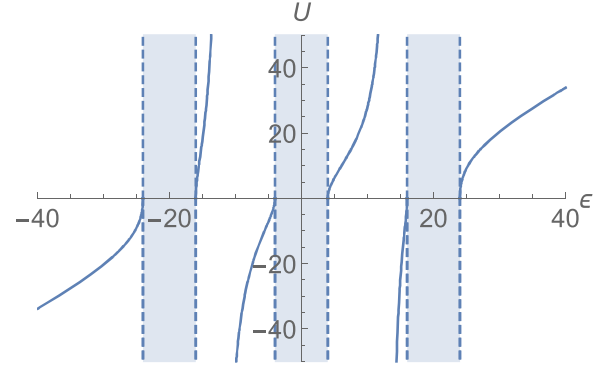


FIG. 4. When $U_2 = 0$ and $U_1 = U$, $\Omega = 10$ and the spectrum possesses three continua, outside of which there are three doublons. The energy ϵ is given in units of J .

essentially superpositions of $|\psi_1\rangle$ and $|\psi_2\rangle$. For instance, if $U_1 = U$ and $U_2 = 0$, we have

$$A_p = \frac{\epsilon - \omega_p - \omega_q - \eta_{pq}}{(\epsilon - \omega_p - \omega_q - \eta_{pq})(\epsilon - \omega_p - \omega_q - \eta_{pq}) - \eta_{pq}^2} \frac{UA}{N}, \quad (38)$$

$$C_p = \frac{\eta_{pq}}{(\epsilon - \omega_p - \omega_q - \eta_{pq})(\epsilon - \omega_p - \omega_q - \eta_{pq}) - \eta_{pq}^2} \frac{UA}{N}, \quad (39)$$

where $\eta_{pq} = \frac{2\Omega^2}{\epsilon - \omega_p - \omega_q}$. We can write the above equations in another form:

$$A_p = \left(\frac{1}{\epsilon - \omega_p - \omega_q - 2\Omega} + \frac{1}{\epsilon - \omega_p - \omega_q + 2\Omega} + \frac{1}{\epsilon - \omega_p - \omega_q} \right) \frac{UA}{2N}, \quad (40)$$

$$C_p = \left(\frac{1}{\epsilon - \omega_p - \omega_q - 2\Omega} + \frac{1}{\epsilon - \omega_p - \omega_q + 2\Omega} - \frac{1}{\epsilon - \omega_p - \omega_q} \right) \frac{UA}{2N}. \quad (41)$$

From these we can deduce that, in the position picture, we have

$$A_{nm} = \lambda'(HC_1 + \lambda HC_2) + HC_0, \quad (42)$$

$$C_{nm} = \lambda'(HC_1 + \lambda HC_2) - HC_0, \quad (43)$$

and

$$B_{nm} = 2\lambda'(HC_1 - \lambda HC_2), \quad (44)$$

where λ and λ' are relative weights to be determined.

The spectrum should then possess three continua, outside of which there are three doublons (see Fig. 4). According to the above wave function and the Schrödinger equations they satisfy,

$$\begin{aligned} \epsilon A + TA + AT - UD_A &= \Omega B_s, \\ \epsilon B + TB + BT &= 2\Omega(A + C), \\ \epsilon C + TC + CT &= \Omega B_s, \end{aligned} \quad (45)$$

we have

$$\lambda'(\tilde{U}_1 s'_1 + \lambda \tilde{U}_2 s'_2) + \tilde{U}_0 s'_0 = U[\lambda'(s'_1 + \lambda s'_2) + s'_0], \quad (46)$$

$$\lambda'(\tilde{U}_1 s'_1 + \lambda \tilde{U}_2 s'_2) - \tilde{U}_0 s'_0 = 0, \quad (47)$$

$$\lambda'(\tilde{U}_1 s'_1 - \lambda \tilde{U}_2 s'_2) = 0, \quad (48)$$

where we have denoted $(1 + s_i)$ by s'_i for convenience. From the three equations, the interaction strength U and the three other fictitious ones \tilde{U}_i can be related via $U = 4/(\frac{2}{\tilde{v}_0} + \frac{1}{\tilde{v}_1} + \frac{1}{\tilde{v}_2})$, similar to the previous example. This result is also confirmed by the numerical solution of the momentum-space Schrödinger equation; see Eq. (A10) for the relation between ϵ and U , which allows us to numerically obtain U given ϵ .

Furthermore, we notice that the antisymmetric solutions (B_a) of the Schrödinger equations still remain when having arbitrary U_1 and U_2 , because their A and C components are zero. Their wave functions and energies do not vary with any interaction. Then we can conclude that when two coupled Bose-Hubbard models have the same single-particle dispersion, there will be three types of two-excitation states in general. Two of the three types are combinations of three different Choy-Haldane states, and the remaining type contains antisymmetrized states with two atoms belonging to two different species. The doublon states are of the former two types.

C. Generic case

Using the insight from the simple, though already nontrivial, cases that we have just studied, we now move on to the generic case of the coupled BHM, anticipating that the solutions are basically superposition of different Choy-Haldane states. We consider arbitrary intraspecies interactions U_1 and U_2 and generally different hopping strengths J_1 and J_2 for the two respective species or copies of the BHM. (The interspecies interaction is not considered here in this section, but the solution to include it can be straightforwardly generalized; see Appendix B.)

First we recall that the Schrödinger equations for this general case are

$$\epsilon A + T_1 A + A T_1 - U_1 D_A = \frac{\Omega}{2} (B + B^T), \quad (49a)$$

$$\epsilon B + T_1 B + B T_2 = 2\Omega (A + C), \quad (49b)$$

$$\epsilon C + T_2 C + C T_2 - U_2 D_C = \frac{\Omega}{2} (B + B^T). \quad (49c)$$

We assume that there is a Choy-Haldane state HC with momenta k and q that is in A , denoted by $\lambda HC \subset A$, and that there is another corresponding term $\lambda' HC \subset C$ with the same k and q . We would like to deduce how the weights λ and λ' are related. We ignore the diagonal part for now, because the diagonal parts of different Choy-Haldane states could be recombined as done in Eq. (31). Then, from the equality of (49a) and (49c) (via the B part) we can relate these two weights,

$$(\epsilon - \omega_k - \omega_q)\lambda = (\epsilon - \omega'_k - \omega'_q)\lambda'. \quad (50)$$

Since the matrix B is not symmetric now, we can separate it into the symmetric and antisymmetric parts

$$B_s = \frac{1}{2}(B + B^T), \quad B_a = \frac{1}{2}(B - B^T). \quad (51)$$

Therefore, there is also a corresponding Choy-Haldane state in B_s as well: $\lambda \frac{\epsilon - \omega_k - \omega_q}{\Omega} HC \subset B_s$.

As the right-hand side (rhs) of the Schrödinger equation (49b) is manifestly symmetric as both A and C are, the left-hand side (lhs) should be so too, which gives

$$\begin{aligned} \epsilon B_s + T_1 B_s + B_s T_2 + \epsilon B_a + T_1 B_a + B_a T_2 \\ = \epsilon B_s + T_2 B_s + B_s T_1 - \epsilon B_a - T_2 B_a - B_a T_1. \end{aligned} \quad (52)$$

We can simplify it to

$$\begin{aligned} 2\epsilon B_a + (T_1 + T_2)B_a + B_a(T_1 + T_2) \\ = (T_2 - T_1)B_s - B_s(T_2 - T_1), \end{aligned} \quad (53)$$

where B_s contains the Choy-Haldane state HC ,

$$HC_{n,m} = \begin{cases} e^{ikn+iqm} + s_{k,q} e^{iqn+ikm}, & n \leq m \\ HC_{m,n}, & n > m, \end{cases} \quad (54)$$

where $s_{k,q} = \frac{2[\sin k_j - \sin(P-k_j)] - i\tilde{u}_i}{2[\sin k_j - \sin(P-k_j)] + i\tilde{u}_i}$ satisfies the corresponding Bethe equation. Substituting it into the right-hand side \mathcal{R} of Eq. (53), we have, for $n < m$,

$$\mathcal{R}_{n,m} = \chi(e^{ikn+iqm} - s_{k,q} e^{iqn+ikm}), \quad (55)$$

where $\chi = \lambda \frac{\epsilon - \omega_k - \omega_q}{\Omega} (\omega_k - \omega'_k - \omega_q + \omega'_q)$.

At this point, it seems natural to introduce a corresponding term in B_a of a similar form in order to make the two sides equal. It is indeed the case with the form

$$HC'_{n,m} = \begin{cases} e^{ikn+iqm} - s_{k,q} e^{iqn+ikm}, & n < m \\ 0, & n = m \\ -HC'_{m,n}, & n > m \end{cases} \quad (56)$$

and we denote the contribution of this Choy-Haldane state to B_a by $\kappa \lambda \frac{\epsilon - \omega_k - \omega_q}{\Omega} HC' \subset B_a$. The weight κ can be determined via Eq. (53),

$$\kappa = \frac{\omega_k - \omega'_k - \omega_q + \omega'_q}{2\epsilon - \omega_k - \omega'_k - \omega_q - \omega'_q}. \quad (57)$$

Then, from the Schrödinger equation (49b) for $n < m - 1$ we have

$$\begin{aligned} \mathcal{L}_{n,m} = \lambda \frac{\epsilon - \omega_k - \omega_q}{\Omega} [(2\epsilon - \omega_k - \omega'_k - \omega_q - \omega'_q) \\ - \kappa(\omega_k - \omega'_k - \omega_q + \omega'_q)](e^{ikn+iqm} + s_{k,q} e^{iqn+ikm}), \end{aligned} \quad (58)$$

$$\mathcal{R}_{n,m} = 4\Omega(\lambda + \lambda')(e^{ikn+iqm} + s_{k,q} e^{iqn+ikm}), \quad (59)$$

where $\lambda + \lambda' = \frac{2\epsilon - \omega_k - \omega'_k - \omega_q - \omega'_q}{\epsilon - \omega'_k - \omega'_q} \lambda$ according to Eq. (50). Equating both sides, we have the consistency equation that involves the energy [see Eq. (7)],

$$\begin{aligned} (2\epsilon - \omega_k - \omega'_k - \omega_q - \omega'_q)^2 - (\omega_k - \omega'_k - \omega_q + \omega'_q)^2 \\ = 4\Omega^2 \frac{(2\epsilon - \omega_k - \omega'_k - \omega_q - \omega'_q)^2}{(\epsilon - \omega_k - \omega_q)(\epsilon - \omega'_k - \omega'_q)}. \end{aligned} \quad (60)$$

The solutions (four of them in general) of this energy equation are exactly a sum of two single-excitation state energies

$$\epsilon = \epsilon_k^\pm + \epsilon_q^\pm, \quad (61)$$

where $\epsilon_k^\pm = [\omega_k + \omega'_k \pm \sqrt{(\omega_k - \omega'_k)^2 + 4\Omega^2}]/2$. However, we emphasize that k and q are quasimomenta instead of physical momenta and their sum is the total momentum P , i.e., $k + q = P$. We remark that when $J_1 = J_2$ and hence $\omega_k = \omega'_k$ (if $\Delta = 0$), Eq. (61), with $U_1 = U_2$, reduces to (a) Eqs. (23) and (24) for the case of $A_{p,q} = C_{p,q}$ and (b) $\epsilon = \omega_k + \omega_{P-k}$ for the case of $A_{p,q} = -C_{p,q}$ in Sec. V A.

Indeed, after specifying the total momentum P , we can have *four* sets of quasimomenta ($k_i, q_i = P - k_i$) in total labeled by the index i for some energy ϵ satisfying Eq. (61). The wave functions of two-excitation eigenstates are combinations of the four corresponding Choy-Haldane states

$$\begin{aligned} A &= \sum_{i=1}^4 \lambda_i H C_i, \\ B &= \sum_{i=1}^4 \lambda_i \frac{\epsilon - \omega_{k_i} - \omega_{q_i}}{\Omega} (H C_i + \kappa_i H C'_i), \\ C &= \sum_{i=1}^4 \lambda'_i H C_i. \end{aligned} \quad (62)$$

There are four equations determining weights λ_i ,

$$\sum_{i=1}^4 J_1 \tilde{u}_i \lambda_i (1 + s_i) = U_1 \sum_{i=1}^4 \lambda_i (1 + s_i), \quad (63)$$

$$\sum_{i=1}^4 J_2 \tilde{u}_i \lambda'_i (1 + s_i) = U_2 \sum_{i=1}^4 \lambda'_i (1 + s_i), \quad (64)$$

$$\sum_{i=1}^4 \kappa_i \lambda_i (\epsilon - \omega_{k_i} - \omega_{q_i}) (1 - s_i) = 0, \quad (65)$$

$$\sum_{i=1}^4 \lambda_i (\epsilon - \omega_{k_i} - \omega_{q_i}) [(J_1 + J_2) \tilde{u}_i (1 + s_i) - (J_1 - J_2) 2i (\sin k_i + \sin q_i) \kappa_i (1 - s_i)] = 0. \quad (66)$$

The virtual interaction strength \tilde{u}_i (for $i = 1, 2, 3, 4$) depends on the quasimomentum k_i and the total momentum P via the Bethe equations. While the nondiagonal entries of the matrix Schrödinger equations give us energy equations (61), as we have seen above, these four equations regarding λ 's come from the almost diagonal entries ($n = m$ and $n = m - 1$) of the Schrödinger equations.

To recapitulate, we show that from a specific energy ϵ , we obtain four sets of quasimomenta $\{k_i, q_i\}$. The total two-particle wave function is composed of four Choy-Haldane states, each having a set of quasimomenta $\{k_i, q_i\}$ and each with a weight λ_i determined by the above equations. In the meantime, we see four continua in the two-particle spectrum (two of the four continua coincide). There is, however, one exception in this description: When $P = 0$, instead of four sets of solutions, we only have three sets of solutions from Eq. (61). This is due to the fact that the two quasimomenta are opposite $q = P - k = -k$, and thus the four equations in

Eq. (61) are not all independent:

$$\epsilon_k^+ + \epsilon_{-k}^- \equiv \epsilon_k^- + \epsilon_{-k}^+. \quad (67)$$

When $P = 0$, it turns out that besides the states in the form $\sum_i H C_i$, there are also antisymmetric solutions of B (with $A = C = 0$) as we saw earlier when $J_1 = J_2$. We now check this statement. The reduced equations for B by taking $A = C = 0$ become

$$2\epsilon B_a + (T_1 + T_2) B_a + B_a (T_1 + T_2) = 0, \quad (68)$$

$$(T_1 - T_2) B_a - B_a (T_1 - T_2) = 0. \quad (69)$$

When $T_1 \neq T_2$, these two equations can be replaced by [as $T_1 = (J_1/J_2)T_2$]

$$(T_1 + T_2) B_a = -\epsilon B_a, \quad (70)$$

$$B_a (T_1 + T_2) = -\epsilon B_a. \quad (71)$$

The matrix $T_1 + T_2$ has eigenvalues $\lambda = -2(J_1 + J_2) \cos k$, where $k = \frac{2r\pi}{N}$, with $r = 1, \dots, N$. So when $k \neq 0, \pi$, there is degeneracy: (e^{ik}, \dots, e^{iNk}) and $(e^{-ik}, \dots, e^{-iNk})$ are distinct solutions but have the same eigenvalue with respect to $T_1 + T_2$. Therefore, we can take the antisymmetric direct product of the two vectors to form a solution of the above matrix equations

$$(B_a)_{i,j} = \sin[(i - j)k]. \quad (72)$$

This solution corresponds to two particles where one has momentum k and the other $-k$, and thus we have a continuum formed by antisymmetric states when the total momentum $P = k + (-k) = 0$.

The existence of this continuum can also be understood as follows. When $P = 0$, from Eq. (57) we have $\kappa = 0$, as $\omega_k = \omega_{-k}$, and that Eq. (53) reduces to $(T_1 - T_2) B_s = B_s (T_1 - T_2)$. Thus the wave-function components in B of Eq. (62) will have a vanishing antisymmetric part. As we obtain three independent solutions from Eq. (61), the number of continua in the form of combinations of Choy-Haldane states is reduced from 4 to 3. Meanwhile, we have antisymmetric states shown in Eq. (72). In total we still have $3 + 1 = 4$ sets of continua when $N \rightarrow \infty$.

When $P \neq 0$, there are four continua formed by combinations of Choy-Haldane states. So when $P \neq 0$, the antisymmetric B_a itself is no longer the eigenstate of the system. Instead, as $\kappa \neq 0$, it becomes a component in the Choy-Haldane form of wave functions as in Eq. (62), which makes the number of such continua 4. Note that what happens in the $J_1 = J_2$ case is that $\kappa \equiv 0$ for all P because $\omega_k \equiv \omega'_k$. Thus the B_a continuum independently exists for all P , as we saw earlier in Sec. V A.

I. Example

We now give an explicit spectrum of the system when $J_1 = 0$, $U_1 = 100J_2$, $\Omega = J_2$, $\Delta = J_2$, and $U_2 = 0$ in Fig. 5. Notice that the middle continuum has a darker shade than the other two, as it represents (effectively) two continua. These two continua of the four coincide, while the doublons appear in between different continua, plotted as red solid lines. The third doublon has a very high energy ($\epsilon \approx 100J_2$) and its

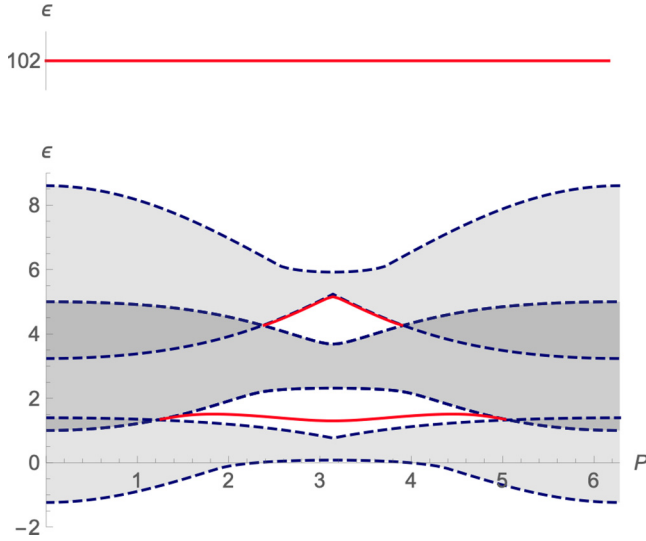


FIG. 5. Spectrum of the two-particle states for $J_1 = 0$, $U_1 = 100J_2$, $U_2 = 0$, and $\Delta = \Omega = J_2$. The red solid curves represent the dispersion for doublons. The energy ϵ is given in units of J_2 . The third doublon is around $\epsilon \approx 102.2J_2$ (shown on top) and its momentum dependence is extremely weak

dispersion is almost flat. We note that similar plots were also shown in Ref. [24], in which the authors used perturbations to acquire the two-particle spectrum.

In this case, since $J_1 = 0$, we have three sets of solutions and three corresponding Choy-Haldane states to combine. However, different from the $P = 0$ case, where we also have three sets of solutions, the number of continua in the spectrum is still 4. The reason is that, in the $P = 0$ case, two solutions of the energy equations coincide, while when J_1 approaches 0, one of the four solutions moves to ∞ . When the quasimomentum k goes to ∞ , the Choy-Haldane state *does not* disappear, but its weight λ for every eigenstate goes to 0. Therefore, the number of continua does not change and remains 4.

2. Including the interspecies interaction

We can also generalize our method discussed in this section to include the interspecies interaction. The steps are similar and the results are presented in Appendix B.

VI. DOUBLON STATES

As mentioned earlier, we call the states outside the continua doublon states. In the single-species Bose-Hubbard model, there is one state outside the continuum. From Eq. (15), in the thermodynamic limit, $U = \pm 4J \cos \frac{P}{2} \sinh K$, and from the energy equation $\epsilon = \pm 4J \cos \frac{P}{2} \cosh K$. In the limit of $U \rightarrow \infty$, this state represents two atoms residing on the same site and traveling through the lattice with momentum P . Thus, this state is called a doublon and can be regarded as one particle with the dispersion relation $\epsilon = \pm \sqrt{U^2 + 16J^2 \cos^2 \frac{P}{2}}$.

With our analytic results in the preceding section, we can easily study doublons in the case of the coupled Bose-Hubbard model. When $N \rightarrow \infty$, the doublon states

have the following real-space wave functions, e.g., the components of A :

$$A_{n,m} = \sum_{i=1}^4 \lambda_i \exp(-K_i |n - m|). \quad (73)$$

As an illustration, we focus on the properties of doublons in the limit of infinite interactions (i.e., U_1 and U_2 being very large). In the general case ($J_1 \neq J_2$), from the Schrödinger equations we have

$$\begin{aligned} \sum_{i=1}^4 J_1 \tilde{u}_i \lambda_i &= U_1 \sum_{i=1}^4 \lambda_i, \\ \sum_{i=1}^4 J_2 \tilde{u}_i \lambda'_i &= U_2 \sum_{i=1}^4 \lambda'_i, \\ \sum_{i=1}^4 \lambda_i (\epsilon - \omega_{k_i} - \omega_{q_i}) [(J_1 + J_2) \tilde{u}_i \\ &\quad - (J_1 - J_2) 2i (\sin k_i + \sin q_i) \kappa_i] = 0, \\ \sum_{i=1}^4 \kappa_i \lambda_i (\epsilon - \omega_{k_i} - \omega_{q_i}) &= 0. \end{aligned} \quad (74)$$

When $U_1 \rightarrow \infty$, the rhs of the first equation must vanish. Therefore, $\sum_i \lambda_i \rightarrow 0$. Two of the three doublon dispersions have finite energies in this limit, their diagonal parts of A in the wave function vanish, and diagonal parts of B and C are the dominant components of the wave functions. When $U_2 \rightarrow \infty$ as well, the diagonal parts of A and C will both vanish for the one of the three doublon dispersions that still has finite energy, while the diagonal parts of B dominate the wave functions,

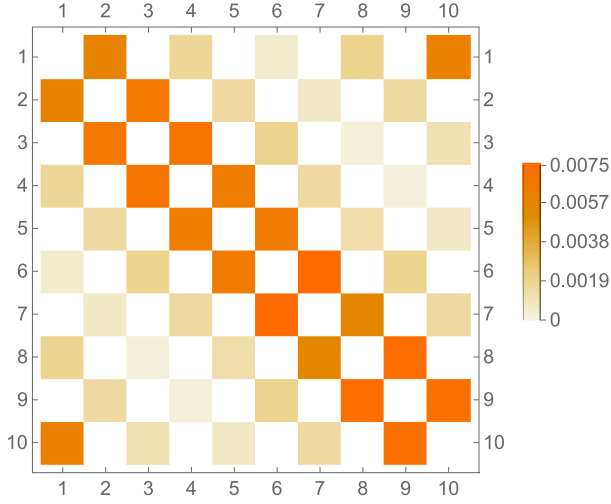
$$B_{n,m} = \sum_{i=1}^4 \lambda_i'' [1 + \kappa_i \text{sgn}(n - m)] \exp(-K_i |n - m|), \quad (75)$$

where $\lambda_i'' \equiv \lambda_i \frac{\epsilon - \omega_{k_i} - \omega_{q_i}}{\Omega}$. We show in Fig. 6 the probability density from the wave function for $U_1 = U_2 \rightarrow \infty$, which clearly demonstrate the adjacency feature.

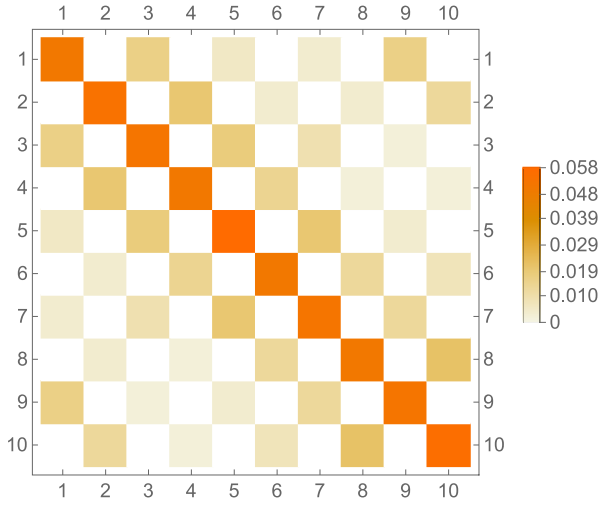
We saw in the preceding section that the number of solutions of energy equations can be deduced by the number of independent linear equations on λ_i . The number of continua can be further inferred. While the number of doublons is set equal to 3, their asymptotic energy as interactions become large can be simply derived. When U_1 and U_2 are large, in the leading order we can ignore the hopping strength J_i . Then the matrix equations are reduced to scalar equations,

$$\begin{pmatrix} \epsilon - U_1 & -\Omega & \\ -2\Omega & \epsilon & -2\Omega \\ & -\Omega & \epsilon - U_2 \end{pmatrix} \begin{pmatrix} a \\ b \\ c \end{pmatrix} \approx 0. \quad (76)$$

If U_1 and U_2 are both large, two doublons will have energies U_1 and U_2 and the other one has a finite energy. If $U_2 = 0$ and U_1 is large, one doublon will have energy U_1 and the other two have a finite energy. We saw these two cases in Sec. V. We can also study the leading-order energy of the three doublons when including interspecies interaction and $\Omega \gg J$ in this way.



(a)



(b)

FIG. 6. Matrix plot of a finite-energy doublon state when $U_1 = U_2 \rightarrow \infty$ and $\Omega/J = 2$, in which case when the diagonal entries of A and C are 0: (a) $|A_{ij}|^2$ (or $|C_{ij}|^2$) and (b) $|B_{ij}|^2$. We set $N = 10$ for the plot.

VII. DETAILED ANALYSIS OF THE DISCRETE SPECTRUM

In this section we describe all two-excitation eigenstates and examine their properties, such as the inverse participation ratio and entanglement behavior. To do this in detail, we will focus on certain limits of the interaction.

When $U_1 = U_2 = U \rightarrow \infty$, we have three types of solutions: (i) ψ_1 , where $A = -C$ is a Choy-Haldane state (with $s_{k,-k} = -1$) and $B = 0$, with the energy $\epsilon = 2\omega_k$; (ii) ψ_2 , where $A = C = HC_1 + \lambda HC_2$ and $B = 2(HC_1 - \lambda HC_2)$, with the energy equation being $\epsilon = 2\omega_{k_1} + 2\Omega = 2\omega_{k_2} - 2\Omega$; and (iii) ψ_3 , which are antisymmetrized states, which will not be of our concern. The first type is a single Choy-Haldane state. When $U \rightarrow \infty$, from the Bethe equation $e^{-ikN} = -1$, the quasimomentum $k = \frac{2\pi}{N} \times$ (half integer).

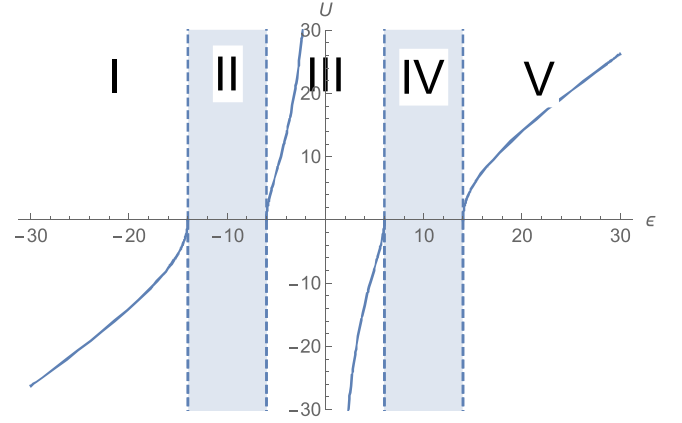


FIG. 7. Spectrum of the second type of state, which can be divided into five parts. This is the spectrum for $P = 0$ specifically.

The second type of state contains two Choy-Haldane states. It was shown in the preceding section that the spectrum of this type of state possesses two continua and two doublon dispersions. We divide the spectrum into five parts as in Fig. 7 and discuss them one by one. We note that the spectrum is different when $\Omega/J < 2$, in which case the two continua overlap. In this case, the only qualitative difference is in region III: Instead of having a localized doublon state, there are additional extended states in the overlapping continuum in region III.

The following are the eigenenergies and the wave functions. In region I,

$$\begin{aligned} \epsilon &= -4 \cos \frac{P}{2} \cosh K_1 + 2\Omega \\ &= -4 \cos \frac{P}{2} \cosh K_2 - 2\Omega \end{aligned} \quad (77)$$

and

$$\begin{aligned} A &= C = HC_1 + \lambda HC_2, \\ B &= 2(HC_1 - \lambda HC_2), \end{aligned} \quad (78)$$

where $\lambda = -\frac{1+s_1}{1+s_2} = -\frac{1+e^{-i(P/2-iK_1)N}}{1+e^{-i(P/2-iK_2)N}}$. When $U \rightarrow -\infty$, K_1 and $K_2 \rightarrow \infty$; when $U \rightarrow +\infty$, there is no solution.

In region II,

$$\begin{aligned} \epsilon &= -4 \cos \frac{P}{2} \cosh K + 2\Omega \\ &= -2 \cos k - 2 \cos(P - k) - 2\Omega \end{aligned} \quad (79)$$

and

$$\begin{aligned} A &= C = HC_1 + \lambda HC_2, \\ B &= 2(HC_1 - \lambda HC_2), \end{aligned} \quad (80)$$

where $\lambda = -\frac{1+s_1}{1+s_2} = -\frac{1+e^{-ikN}}{1+e^{-i(P/2-iK)N}}$. When $U \rightarrow +\infty$, $\tilde{u}_1 = -\tilde{u}_2$, whose expressions are

$$\begin{aligned} \tilde{u}_1 &= 2[\sin k - \sin(P - k)] \tan \frac{kN}{2}, \\ \tilde{u}_2 &= -4i \cos \frac{P}{2} \sinh K \tan\left(\frac{P}{2} - iK\right) \frac{N}{2}. \end{aligned} \quad (81)$$

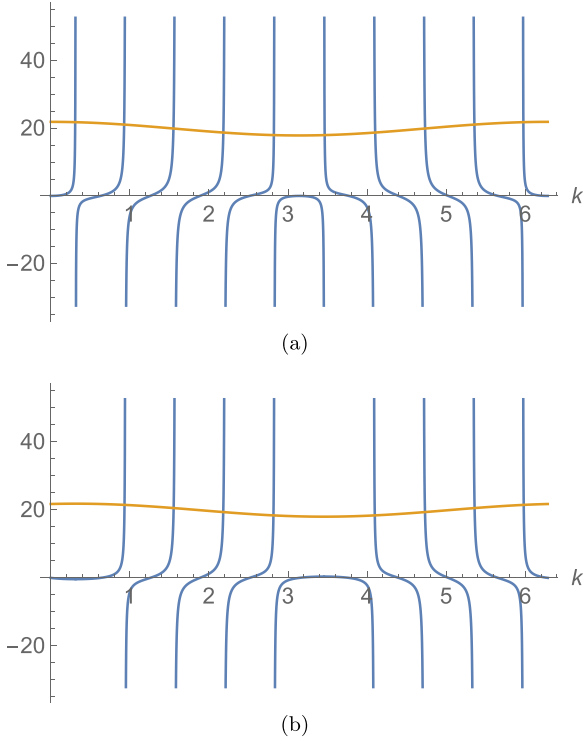


FIG. 8. Solution of $\tilde{u}_1 = -\tilde{u}_2$ in Eq. (81). (a) The blue (yellow) curve is the lhs (rhs) of the equation in terms of k when $P = 0$, for $N = 10$ type-2 states in region II. (b) The blue (yellow) curve is the lhs (rhs) of the equation in terms of k when $P = \frac{2\pi}{10}$, for $N = 10$ type-2 states in region II. Every intersection of the two curves gives one such state.

Given a total site number N , the total momentum can be $P = \frac{2\pi r}{N}$, with $r = 0, 1, \dots, N-1$. For each P value, the above equations could be solved numerically. For instance, we take $N = 10$ and $\Omega = 10J$. When $P = 0$, we plot in Fig. 8(a) the lhs and rhs of the equation $\tilde{u}_1 = -\tilde{u}_2$ in terms of k .

Thus the equations have five solutions, if we consider the fact that by exchanging k and $P - k$, we essentially have the same state. The corresponding plot for $P = \frac{2\pi}{10}$ is shown in Fig. 8(b). There are four solutions in this case. This pattern persists if we continue with higher P . When r is even, we would have five distinct states, but when r is odd, we would have only four distinct solutions. In total, when $N = 10$, region II of the second type gives 55 states.

In region III,

$$\begin{aligned} \epsilon &= -4 \cos \frac{P}{2} \cosh K_1 + 2\Omega \\ &= 4 \cos \frac{P}{2} \cosh K_2 - 2\Omega \end{aligned} \quad (82)$$

and

$$\begin{aligned} A &= C = HC_1 + \lambda HC_2, \\ B &= 2(HC_1 - \lambda HC_2), \end{aligned} \quad (83)$$

where $\lambda = -\frac{1+s_1}{1+s_2} = -\frac{1+e^{-i(P/2-iK_1)N}}{1+e^{-i(\pi+P/2-iK_2)N}}$. When $U \rightarrow +\infty$ and $\epsilon = 0$, the equation $\tilde{u}_1 = -\tilde{u}_2$ is satisfied automatically. The

energy equations become $2 \cos \frac{P}{2} \cosh K = \Omega$, where $K_1 = K_2 = K$:

$$\tilde{u}_1 = -4i \cos \frac{P}{2} \sinh K \tan \left[\left(\frac{P}{2} - iK \right) \frac{N}{2} \right], \quad (84)$$

$$\tilde{u}_2 = 4i \cos \frac{P}{2} \sinh K \tan \left[\left(\pi + \frac{P}{2} - iK \right) \frac{N}{2} \right]. \quad (85)$$

We note that the factor $\tan \left[\left(\frac{P}{2} - iK \right) \frac{N}{2} \right] = \tan \left[\left(\pi + \frac{P}{2} - iK \right) \frac{N}{2} \right]$ for any N , and therefore $\tilde{u}_1 = -\tilde{u}_2$. There is one state for each P , thus ten states in total.

If the two continua II and IV overlap, as long as $\Omega \neq 0$, the above equations will still give us some valid wave functions. However, in this case we would expect some extended states in the overlapped region, whose quasimomenta are real,

$$\begin{aligned} \epsilon &= -2 \cos k_1 - 2 \cos(P - k_1) - 2\Omega \\ &= -2 \cos k_2 - 2 \cos(P - k_2) + 2\Omega, \end{aligned} \quad (86)$$

while

$$\begin{aligned} \tilde{u}_1 &= 2[\sin k_1 - \sin(P - k_1)] \tan \frac{k_1 N}{2}, \\ \tilde{u}_2 &= 2[\sin k_2 - \sin(P - k_2)] \tan \frac{k_2 N}{2}. \end{aligned} \quad (87)$$

In region IV,

$$\begin{aligned} \epsilon &= -2 \cos k - 2 \cos(P - k) + 2\Omega \\ &= 4 \cos \frac{P}{2} \cosh K - 2\Omega \end{aligned} \quad (88)$$

and

$$\begin{aligned} A &= C = HC_1 + \lambda HC_2, \\ B &= 2(HC_1 - \lambda HC_2), \end{aligned} \quad (89)$$

where $\lambda = -\frac{1+s_1}{1+s_2} = -\frac{1+e^{-i(\pi+P/2-iK)N}}{1+e^{-iK N}}$. When $U_1 \rightarrow +\infty$, $\tilde{u}_1 = -\tilde{u}_2$, where

$$\begin{aligned} \tilde{u}_1 &= -4i \cos \frac{P}{2} \sinh K \tan \left(\frac{P}{2} - iK \right) \frac{N}{2}, \\ \tilde{u}_2 &= 2[\sin k - \sin(P - k)] \tan \frac{kN}{2}. \end{aligned} \quad (90)$$

As in region II, there are 55 states in total when $N = 10$.

In region V,

$$\begin{aligned} \epsilon &= 4 \cos \frac{P}{2} \cosh K_1 + 2\Omega \\ &= 4 \cos \frac{P}{2} \cosh K_2 - 2\Omega \end{aligned} \quad (91)$$

and

$$\begin{aligned} A &= C = HC_1 + \lambda HC_2, \\ B &= 2(HC_1 - \lambda HC_2), \end{aligned} \quad (92)$$

where $\lambda = -\frac{1+s_1}{1+s_2} = -\frac{1+e^{-i(\pi+P/2-iK_1)N}}{1+e^{-i(\pi+P/2-iK_2)N}}$. When $U_1 \rightarrow +\infty$, K_1 and $K_2 \rightarrow \infty$.

In regions III and V, the eigenvalues are straightforwardly obtained. In regions II and IV, we need to solve for the two quasimomenta satisfying both energy equations and the equation $\tilde{u}_1 = -\tilde{u}_2$, as illustrated in Fig. 8.

Now with solutions of all two-particle eigenstates, we examine them in terms of their inverse participation ratio.

Inverse participation ratio. We use the inverse participation ratio (IPR) \mathcal{I} to characterize and demonstrate the localization properties of all the eigenstates [54]. The IPR in the single-particle case is defined as the integral of the square of the density over the space, i.e., $\mathcal{I} = \sum_i |\psi_i|^4$. In our system we choose a two-particle spatial basis to define the IPR, which is a special case of the many-body IPR (see, e.g., Ref. [47]) and we obtain

$$\mathcal{I} = \sum_{n,m} 4|A_{n,m}|^4 + |B_{n,m}|^4 + 4|C_{n,m}|^4, \quad (93)$$

under our previous normalization in Eq. (28). For the case of $N = 10$ and $U_1 = U_2 = \infty$, Fig. 9 shows the whole spectrum of type-2 states. When $\Omega/J = 10$, states in the two continua are pretty much extended ($\mathcal{I} < 0.01$) and the doublon states are highly localized ($\mathcal{I} \approx 0.1$, which is the largest IPR of states under translational symmetry).

When $\Omega/J = 1$, the two continua intersect around $\epsilon = 0$. The doublon states thus vanish, replaced by the more extended states in region III. These eigenstates are composed of two Choy-Haldane states with real quasimomenta, i.e., they are essentially combinations of scattering states. Therefore, their IPRs are expected to be lower than all the other states.

Therefore, we observe a hierarchy of localization in the spectrum. The most localized states are the doublons, followed by the states composed of one scattering state and one localized state, and then the states composed of two scattering states, which are the most delocalized among the three kinds. Note that the doublon in between two continua and the states of the third kind cannot appear simultaneously. When Ω is large, the two continua are distant and the doublon emerges in between as the interaction is turned on; when Ω is small, the two continua intersect and the doublon is replaced by the scattering states. We note that since the IPR just depends on the density distribution of the system, it can in principle be measured by imaging the system [55].

Entanglement. We also calculate the entanglement between the two species a and b . To do this, we define the reduced density matrix ρ_a for species a by tracing over the degrees of freedom in b -particle Hilbert space. Given that there are at most two b particles, we have ρ_a for a given two-excitation state $|\psi\rangle$ defined as

$$\begin{aligned} \rho_a = & {}_b\langle 0|(|\psi\rangle\langle\psi|)|0\rangle_b + \sum_i {}_b\langle 0|b_i|\psi\rangle\langle\psi|b_i^\dagger|0\rangle_b \\ & + \sum_{ij} \frac{1}{2} {}_b\langle 0|b_j b_i|\psi\rangle\langle\psi|b_i^\dagger b_j^\dagger|0\rangle_b, \end{aligned} \quad (94)$$

where we have used $|0\rangle_b$ to define the vacuum for b particles. We expect that ρ_a will be block diagonal with three blocks contributed by the vacuum and one-particle and two-particle subspaces, respectively,

$$\rho_a = \rho_2 \oplus \rho_1 \oplus \rho_0. \quad (95)$$

The entanglement entropy of $|\psi\rangle$ is then given by

$$S_{\text{VN}} = -\text{Tr}(\rho_a \ln \rho_a) = S_2 + S_1 + S_0, \quad (96)$$

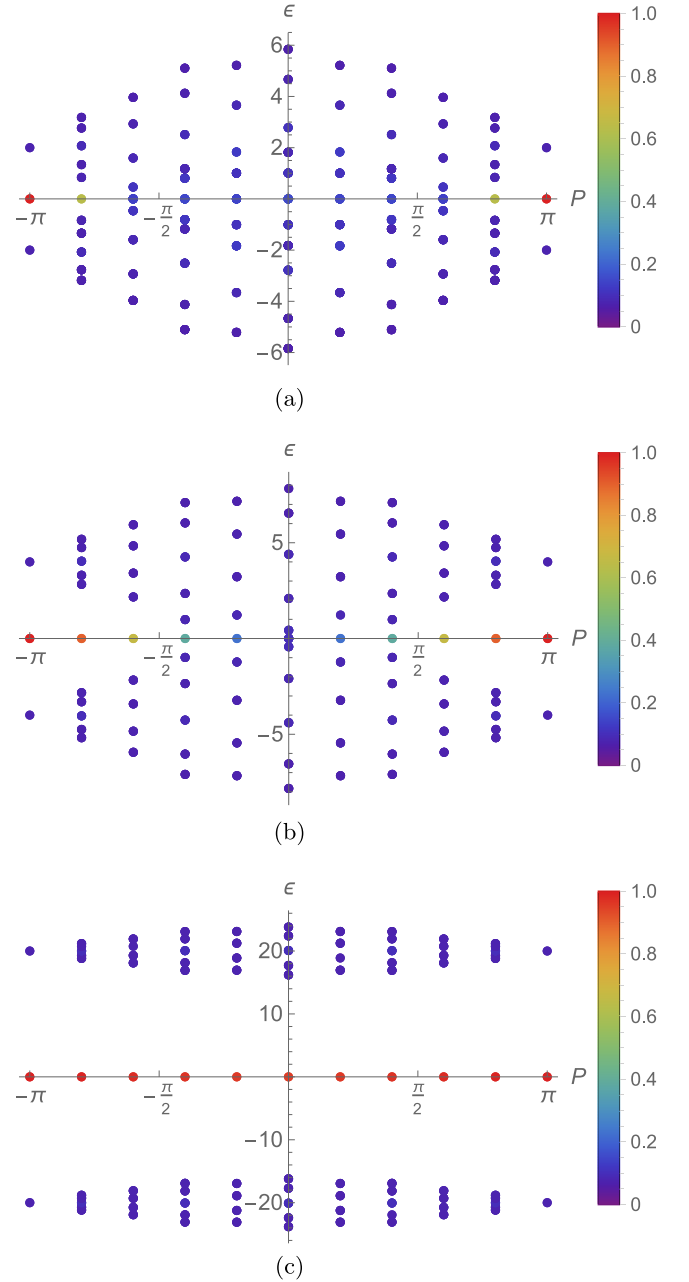


FIG. 9. Spectrum ϵ and IPR (represented by color) of type-2 states vs momentum P when $U_1 = U_2 = U \rightarrow \infty$. (a) For $\Omega/J = 1$, two continua overlap and all the states in the continua including those inside the overlapped region are extended. (b) For $\Omega/J = 2$, two continua lie side by side. The doublon states become more localized when they are energetically distant from those in the continua. (c) For $\Omega/J = 10$, the doublon states are almost maximally localized. Their IPR reaches 0.1, which is the maximal value assuming translational invariance. The total site number is taken to be $N = 10$

where $S_i \equiv -\text{Tr}(\rho_i \ln \rho_i)$. To be more specific, we have

$$S_2 = -\lambda_c \ln \lambda_c, \quad (97)$$

$$S_1 = -\text{Tr}(BB^\dagger \ln BB^\dagger), \quad (98)$$

$$S_0 = -\lambda_a \ln \lambda_a, \quad (99)$$

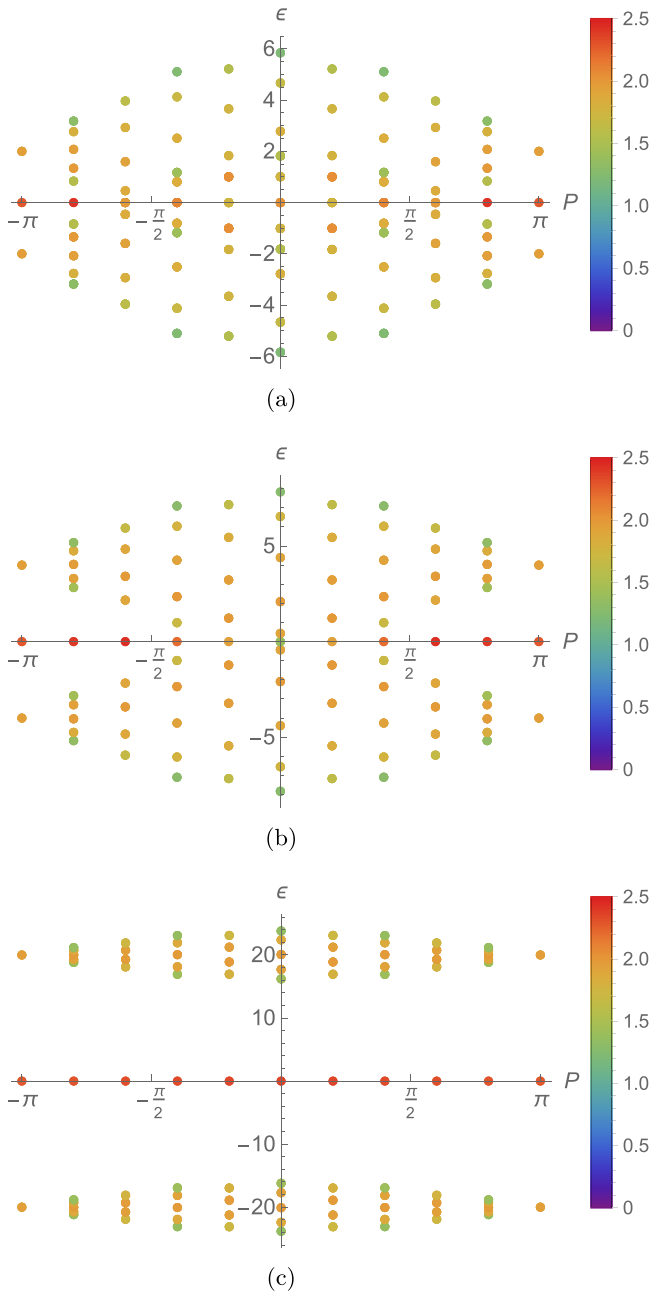


FIG. 10. Entanglement entropy of type-2 states when $U_1 = U_2 = U \rightarrow \infty$. (a) For $\Omega/J = 1$ two continua overlap. The states in the overlapped region have slightly higher entanglement between particles a and b . (b) For $\Omega/J = 2$, two continua lie side by side. The doublon states have an entanglement entropy that is close to $\ln 2$. (c) For $\Omega/J = 10$, the doublon states are at almost maximal (approximately equal to $\ln 10$) entanglement between particles a and b . States on the edge of each continuum have slightly lower entanglement than the other states in the continuum. The total site number is taken to be $N = 10$

where $\lambda_a \equiv \sum_{n,m} 2|A_{n,m}|^2$ and $\lambda_c \equiv \sum_{n,m} 2|C_{n,m}|^2$. For type-1 eigenstates, $A = -C$ and $B = 0$. After imposing normalization as in Eq. (28), we have $\lambda_a = \lambda_c = \frac{1}{2}$. Thus the entanglement entropy of type-1 eigenstates is $\bar{S} = \ln 2$. We show the entanglement entropy of type-2 states in Fig. 10.

Site number. The analysis for now in this part concentrates on the system with $N = 10$ sites for simplicity and for illustration. If we increase N , the number of states will increase for sure. Other than that, the IPR of doublon state will scale as $\sim 1/N$, while the IPR of states in the continua will scale as $\sim 1/N^2$. The entropy of doublon states will be $\sim \ln N$ and the entropy of other states will be much lower. Eventually, when the thermodynamic limit is reached, states form four real continua (one in type 1, two in type 2, and one in type 3).

VIII. TIME EVOLUTION

After analyzing detailed eigenstates in Sec. VII, it is natural to ask how the system evolves from a certain initial state. To write down the total wave function, we start with four sets of quasimomenta which satisfy their corresponding energy equations. Then using the Bethe equations and equations recombining diagonal parts, we can determine the \tilde{u} , $s_{k,q}$, and λ . After writing out the complete basis set, for every initial state (e.g., $B_{nm} = \delta_{n,0}\delta_{m,0}$), we can expand the total wave function in terms of the eigenbasis. After the expansion, we obtain the time evolution of the system easily: $|\psi(t)\rangle = \sum_i c_i e^{-iE_i t} |E_i\rangle$. This approach applies to arbitrary long times. We also remark that we also integrate the time-dependent Schrödinger equation numerically to obtain the dynamics, which is good for time not too long so that the numerical error does not accumulate too much.

To study the time evolution of a system that possesses doublon dispersions, we set the initial state to be $|\psi\rangle = a_0^\dagger b_0^\dagger |0\rangle$, with two bosons of different species occupying the same position, and examine the case when $U_1 = U_2 = U$ is large. From the flat dispersion of the doublon state, we expect the initial state to persist in the large- Ω and large- U limit. Therefore, we examine the time evolution of $N_{\text{db}} \equiv \sum_i |\langle \psi | a_i^\dagger b_i^\dagger a_i b_i | \psi \rangle|^2$, which counts only the double occupation of different species at the same sites. The initial value $N_{\text{db}} = 1$, as shown in Fig. 11, and it decays incompletely and persists at a high value at late times.

To study the mean and fluctuations of N_{db} for a broader range of Ω/J , we plot these values gathered between times $t = 30$ and 40 in Fig. 12. When $\Omega/J < 2$, although doublon states exist near $P = \pi$ in the momentum space, two continua overlap around $P = 0$. As a result, N_{db} decays drastically, giving a small mean and large deviation in the plot. When $\Omega/J > 2$, once the doublon has a full band, the time evolution of N_{db} is dominated by the doublon. This phenomenon is due to the localization property of doublon states; thus when Ω is small enough such that doublons do not exist, we expect a pretty different late-time behavior. The difference in the late-time behavior due to doublon states can be observed in the time evolution of the IPR. When $\Omega/J < 2$, the IPR will drastically decrease from 1 to 0 and oscillate slightly above it. When $\Omega/J > 2$, the IPR will decrease from 1 to somewhere above $1/N$ (which is 0.1 in our case study) instead.

Note that when $U \rightarrow \infty$ and $\Omega \rightarrow \infty$, due to the flat doublon dispersion, the initial state is an eigenstate. Both N_{db} and the IPR will remain 1 in the unitary evolution and we have a standing doublon. When $U \rightarrow \infty$ and $\Omega \gg 1$, doublon dispersion is not perfectly flat and N_{db} will be still close to 1, but the IPR will drop as shown in Fig. 13(c).

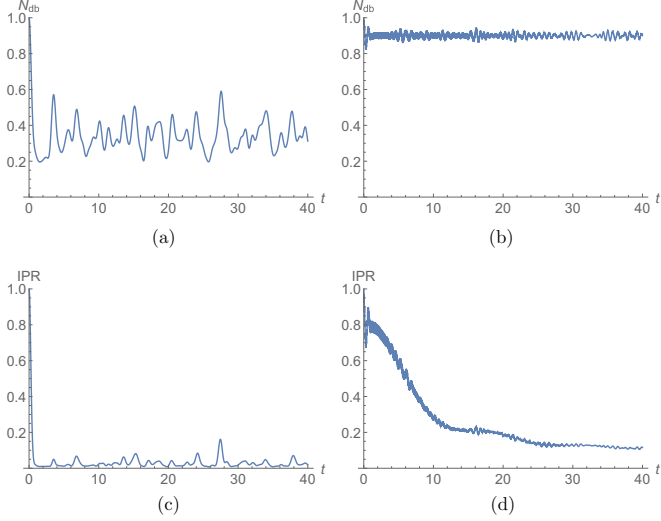


FIG. 11. Time evolution of N_{db} and IPR for $U/J = 100$ and $N = 10$ sites. (a) For $\Omega/J = 1$, N_{db} decays and oscillates drastically. (b) For $\Omega/J = 5$, N_{db} remains slightly smaller than 1. (c) For $\Omega/J = 1$, the IPR decays to around 0.01 and oscillates. (d) For $\Omega/J = 5$, the IPR decays, but has a minimum 0.1. The time t is given in units of $1/J$.

We also study the time evolution of entanglement entropy between a and b particles from the same initial state of $a_0^\dagger b_0^\dagger |0\rangle$ as above. In Fig. 13(a) we show the evolution of the entanglement entropy when $U/J = 500$ and $\Omega/J = 10$. We observe very-high-frequency oscillation, which is easier to see in Fig. 13(e) with $U/J = 100$. This is due to the interference between the doublon state in region III and that in region IV. Therefore, the frequency is proportional to the energy difference $\Delta\epsilon$ between the two states. When $U \gg 1$ and $\Omega \gg U$, $\Delta\epsilon \propto \Omega$; when $U \gg 1$ but $U \gg \Omega$, $\Delta\epsilon \propto U$. This can be seen from comparing Figs. 13(a) and 13(e), where the high-frequency oscillation in the latter is slower than in the former. Moreover, the entropy varies drastically from $Jt = 0$,

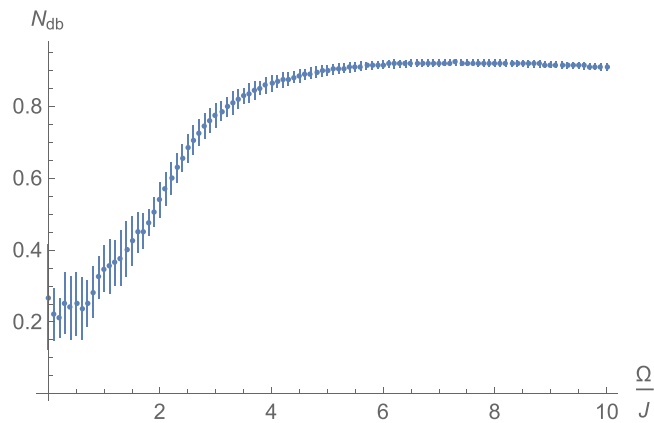


FIG. 12. Mean values and standard deviations of N_{db} between $t = 30$ and 40 for $U/J = 100$. When $\Omega/J > 2$, because of the formation of the doublon, the late time mean is high, with small deviation (oscillation amplitude). When Ω/J is small, the mean is small and the deviation is quite high, indicating a different late-time behavior.

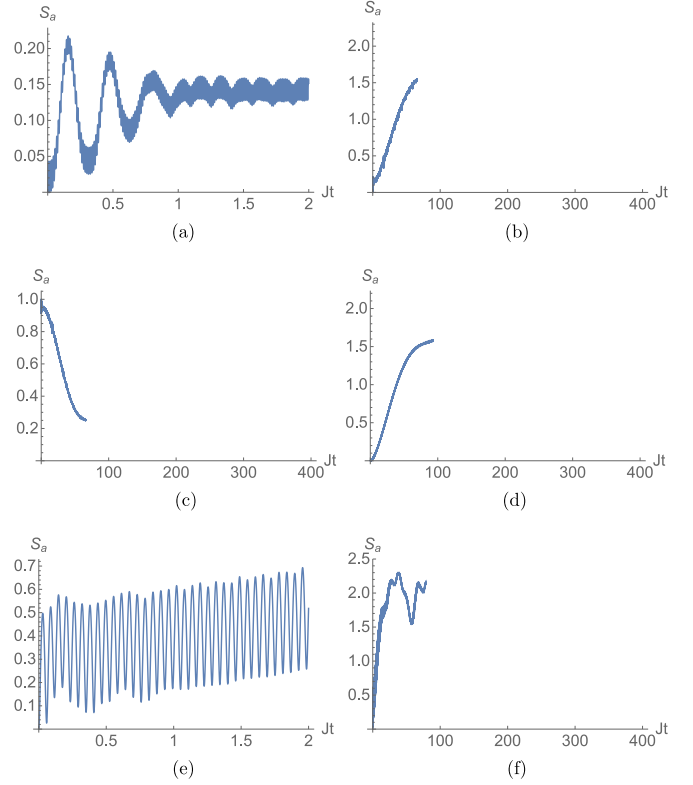


FIG. 13. (a)–(c) Time evolution of the coupled Bose-Hubbard model when $\Omega/J = 10$ and $U/J = 500$. Entanglement entropy evolution is shown from (a) $Jt = 0$ to 2 and (b) $Jt = 0$ to 400. (c) The IPR from $Jt = 0$ to 400. (d) Time evolution of the two-particle state in the single-species Bose-Hubbard model with $U'/J = -166.7$, which is almost identical to that in (b) except for the small-amplitude oscillations and the initial buildup. Entanglement evolution between two particles is shown from (e) $Jt = 0$ to 2 and (f) $Jt = 0$ to 400 when $U/J = 100$. The oscillation pattern in (f) is 5 times faster than that in (b). In (a) an initial buildup of entanglement is shown in a form similar to a damped oscillator. In contrast, such an initial buildup for $U/J = 100$ is weaker, as seen in (e).

analogous to a damped oscillation, and saturates around $Jt \approx O(1)$, with the saturation time dependent on Ω . From then on after the initial buildup, the evolution is milder.

The large-timescale evolution of the entropy is shown in Fig. 13(b) with $U/J = 500$. This behavior is due to the dispersion of the doublon. When $U \gg 1$ and Ω is large, from Eq. (35), the group velocity of the doublon is

$$\frac{d\epsilon}{dP} \approx \frac{1}{U} 12J^2 \sin P. \quad (100)$$

The simple way to demonstrate our claim regarding the behavior of entanglement is to use the single-species Bose-Hubbard model under time evolution. In this case, when the interaction strength $U' \gg 1$ (we add a prime to U to distinguish it from the interaction strengths in the coupled case), using the energy equation $\epsilon = \sqrt{U'^2 + 16J^2 \cos^2 \frac{P}{2}}$, the doublon group velocity is

$$\frac{d\epsilon}{dP} \approx -\frac{1}{U'} 4J^2 \sin P. \quad (101)$$

After the above preparation, we can now study the entanglement entropy evolution between the two particles in the single-species Bose-Hubbard model with $U' = -\frac{U}{3}$ and the initial state being $|\psi\rangle_0 = \frac{1}{\sqrt{2}}a_0^\dagger a_0^\dagger |0\rangle$. The entanglement behavior in the single-species case is expected to be similar to that in the coupled case with $U = -3U'$. The expression (98) for two species motivates us to define the entanglement entropy for the single-species case as $S = -\text{Tr}(AA^\dagger \ln AA^\dagger)$ for the wave function of the form $|\psi\rangle = \sum_{n,m} A_{n,m} a_n^\dagger a_m^\dagger |0\rangle$. As long as $U \gg 1$, we should expect a similar result in both single- and double-species cases, since the doublons in two systems have roughly the same dispersion. We demonstrate this for $U' = -\frac{500}{3}$ (corresponding to $U = 500$) in Fig. 13(d), in which the evolution is essentially the same as in Fig. 13(b), except that in the (single-species) Bose-Hubbard model there is no initial buildup process. Additionally, when U/J is lowered to 100, as in Fig. 13(f) the oscillation pattern is 5 times faster than that in Fig. 13(b). We also see that in Figs. 13(b) and 13(c), when the entropy increases, the IPR decreases and vice versa. This confirms the claim that the large-timescale evolution is due to the dispersion of the doublon. Notice that the IPR oscillates above 0.1 at large times; $\mathcal{I} = 1/N = 0.1$ is the value of the IPR when the probability density is evenly distributed in N lattice sites.

IX. CONCLUSION

We have solved the two-particle spectrum of a generic doubly coupled Bose-Hubbard model. Our solutions include several different two-particle continua and doublon dispersions outside the continua. The continua are composed of states whose wave functions are superpositions of Choy-Haldane states in general. In addition to these extended states, we have also obtained doublon states that are localized (in relative coordinates). These doublons can differ from those in the single-species Bose-Hubbard model in the pattern of spatial occupation (or the adjacency feature referred earlier), such as nearest neighbor vs on site. Some doublons possess energies that overlap with a continuum, and hence they are also bound states in the continuum.

Given that we were able to solve for all two-particle eigenstates, we have examined the inverse participation ratio and entanglement entropy (between the two species) for eigenstates. As doublon states are localized, they do possess a large IPR. They also have a large entanglement between the two species. We have also studied the dynamics of simple initial two-particle states and found that the IPR and entanglement behave in opposite ways under the time evolution of the coupled Bose-Hubbard Hamiltonian. It is interesting that the behavior of entanglement is dominated by doublons at late times, and this is confirmed by the similar single-species Bose-Hubbard case. The correspondence between the coupled

case and the single-species case is identified by a relation in their interactions (e.g., $U = -3U'$) inferred from the doublon dispersions. We remark that our approach can be extended to include next-nearest-neighbor or longer-range hopping and to an arbitrary number of Bose-Hubbard models that are coupled, albeit still only one- and two-particle solutions.

Our paper provides a complete solution for the two-particle subspace; however, finding analytic solutions for many interacting bosons remains challenging. In certain limiting cases, few-particle solutions, such as those with bound states, may offer a qualitative explanation for many-body states in some regime. In Ref. [56] the authors found that the formation of the liquid in the one-dimensional Bose-Hubbard model coincides with the appearance of a bound state in the dimer-dimer problem. Moreover, doublons have been observed in one-dimensional (single-species) Bose-Hubbard experiments in a low filling factor [35]. We expect that when the doublons are localized enough (when Ω is large enough), one could observe the doublons and the effects they have in a sparse lattice. The most obvious method is to image the system using, e.g., a quantum gas microscope [57]. For example, when $U_1 = U_2 \gg 1$, the group velocity of doublons approaches zero, which means that if one carefully specifies the initial state as several doublons lying in a sparse lattice, all the particles will essentially freeze at their initial positions. One could vary the interactions and observe different dynamics. Alternatively, one could also use modulation spectroscopy and time-of-flight techniques to detect the presence of doublons, similar to the single-species case in [35].

Finally, a digital quantum computer may also be used to simulate the system. When $U_1 = U_2 = \infty$, the a and b particles are hard-core bosons. So the two-particle wave function can be simulated by a and b types of qubits, with coupling on site. However, when the intraspecies interaction is finite, the two-particle wave function should be simulated by two types of qutrits instead of qubits, as there are three possible occupations $|0\rangle$, $|1\rangle$, and $|2\rangle$ of the same species. Their dynamics can be studied in principle via a Trotter-Suzuki decomposition of the time-evolution operator into a sequence of quantum gates. The IPR, entanglement (perhaps using the Rényi entropy of order 2 instead of the von Neumann entropy), and diagonal occupation can all be studied by measurements. At the moment, qubit digital quantum computers look more promising for hard-core bosons, but some recent experiments have begun to explore qutrits [58], which might be used to simulate general two-excitation states in the coupled Bose-Hubbard model.

ACKNOWLEDGMENTS

This work was supported by National Science Foundation Grants No. PHY-1915165 (Y.L. and T.-C.W.) and No. PHY-1912546 (D.S.) as well as an SBU seed grant (Y.L., D.S. and T.-C.W.) on the initial design of the project.

APPENDIX A: MOMENTUM-SPACE SCHRÖDINGER EQUATIONS

The following are the momentum-space Schrödinger equations:

$$(\epsilon - \omega_p - \omega_q)A_{p,q} = \frac{U_1}{N} \sum_{p+q=P} A_{p,q} + \frac{\Omega}{2}(B_{p,q} + B_{q,p}), \quad (\text{A1a})$$

$$(\epsilon - \omega_p - \omega'_q)B_{p,q} = 2\Omega A_{p,q} + 2\Omega C_{p,q}, \quad (\text{A1b})$$

$$(\epsilon - \omega'_p - \omega'_q)C_{p,q} = \frac{U_2}{N} \sum_{p+q=P} C_{p,q} + \frac{\Omega}{2}(B_{p,q} + B_{q,p}). \quad (\text{A1c})$$

Substituting (A1c) into (A1b), we have

$$\begin{aligned} (\epsilon - \omega_p - \omega_q)A_{p,q} &= \frac{U_1 A}{N} + \frac{\Omega}{2}(B_{p,q} + B_{q,p}), \\ 2\Omega A_{p,q} &= (\epsilon - \omega_p - \omega'_q)B_{p,q} - \Omega^2 \frac{B_{p,q} + B_{q,p}}{\epsilon - \omega'_p - \omega'_q} + \frac{2\Omega U_2 C}{N(\epsilon - \omega'_p - \omega'_q)}. \end{aligned} \quad (\text{A2})$$

Substituting (A1b) into (A1a), we have

$$\begin{aligned} (\epsilon - \omega_p - \omega'_q)B_{p,q} - \Omega^2 \left(\frac{1}{\epsilon - \omega_p - \omega_q} + \frac{1}{\epsilon - \omega'_p - \omega'_q} \right) (B_{p,q} + B_{q,p}) \\ = \frac{2\Omega U_1 A}{N} \frac{1}{\epsilon - \omega_p - \omega_q} - \frac{2\Omega U_2 C}{N} \frac{1}{\epsilon - \omega'_p - \omega'_q}. \end{aligned} \quad (\text{A3})$$

From Eq. (A2) we could further have

$$\frac{\epsilon - \omega_p - \omega'_q}{2\Omega} B_{p,q} = \frac{2\epsilon - \omega_p - \omega_q - \omega'_p - \omega'_q}{\epsilon - \omega'_p - \omega'_q} A_{p,q} - \frac{U_1 A}{N} \frac{1}{\epsilon - \omega'_p - \omega'_q} - \frac{U_2 C}{N} \frac{1}{\epsilon - \omega'_p - \omega'_q}. \quad (\text{A4})$$

Substituting this into Eq. (A3) and taking advantage of the fact that $A_{p,q} = A_{q,p}$, we arrive at

$$A_{p,q} = \frac{1}{(\epsilon - \omega_p - \omega_q - \eta_{pq})(\epsilon - \omega'_p - \omega'_q - \eta_{pq}) - \eta_{pq}^2} \left((\epsilon - \omega'_p - \omega'_q - \eta_{pq}) \frac{U_1 A}{N} + \eta_{pq} \frac{U_2 C}{N} \right), \quad (\text{A5})$$

where $\eta_{pq} \equiv \Omega^2 \left(\frac{1}{\epsilon - \omega_p - \omega'_q} + \frac{1}{\epsilon - \omega_q - \omega'_p} \right)$. Similarly for $C_{p,q}$,

$$C_{p,q} = \frac{1}{(\epsilon - \omega_p - \omega_q - \eta_{pq})(\epsilon - \omega'_p - \omega'_q - \eta_{pq}) - \eta_{pq}^2} \left(\eta_{pq} \frac{U_1 A}{N} + (\epsilon - \omega_p - \omega_q - \eta_{pq}) \frac{U_2 C}{N} \right). \quad (\text{A6})$$

This essentially forms a matrix equation

$$\begin{pmatrix} A_p \\ C_p \end{pmatrix} = M(p) \begin{pmatrix} \frac{A}{N} \\ \frac{C}{N} \end{pmatrix}. \quad (\text{A7})$$

Since $\sum_p A_p = A$ and $\sum_p C_p = C$, we have an equation for the matrix M which essentially becomes the energy equation

$$\det \left(\sum_p M(p) - \mathbf{1} \right) = 0, \quad (\text{A8})$$

or in the thermodynamic limit, the sum becomes an integral

$$\det \left(\int_0^{2\pi} \frac{dp}{2\pi} M(p) - \mathbf{1} \right) = 0. \quad (\text{A9})$$

As an example, when $U_2 = 0$ and $J_2 = 0$, the matrix equation reduces to an ordinary equation. Then the energy equation is

$$\sum_{p+q=P} \frac{U}{N} \frac{(\epsilon - \omega_p - \omega_q) - \left(\frac{\Omega^2}{\epsilon - \Delta - \omega_q} + \frac{\Omega^2}{\epsilon - \Delta - \omega_p} \right)}{(\epsilon - 2\Delta)(\epsilon - \omega_p - \omega_q) - (2\epsilon - 2\Delta - \omega_p - \omega_q) \left(\frac{\Omega^2}{\epsilon - \Delta - \omega_q} + \frac{\Omega^2}{\epsilon - \Delta - \omega_p} \right)} = 1. \quad (\text{A10})$$

In the limit of $N \rightarrow \infty$, this sum turns into an integral

$$\int_0^{2\pi} dp \frac{(\epsilon - \omega_p - \omega_q) - \left(\frac{\Omega^2}{\epsilon - \Delta - \omega_q} + \frac{\Omega^2}{\epsilon - \Delta - \omega_p} \right)}{(\epsilon - 2\Delta)(\epsilon - \omega_p - \omega_q) - (2\epsilon - 2\Delta - \omega_p - \omega_q) \left(\frac{\Omega^2}{\epsilon - \Delta - \omega_q} + \frac{\Omega^2}{\epsilon - \Delta - \omega_p} \right)} \Bigg|_{q=P-p} = \frac{2\pi}{U}. \quad (\text{A11})$$

From this equation one can in principle solve for the two-excitation energy ϵ . In fact, we can use this in the opposite direction, i.e., by fixing an ϵ and performing the integration (e.g., numerically) to obtain the corresponding interaction U . This allows us to obtain the relation between ϵ and U , in particular, for the doublons.

APPENDIX B: INTERSPECIES INTERACTION

So far we have not included the interaction between the two species of atoms. If we have interspecies interaction, the Schrödinger equations become

$$\epsilon A + T_1 A + AT_1 - U_1 D_A = \frac{\Omega}{2}(B + B^T), \quad (\text{B1})$$

$$\epsilon B + T_1 B + BT_2 - U_3 D_B = 2\Omega(A + C), \quad (\text{B2})$$

$$\epsilon C + T_2 C + CT_2 - U_2 D_C = \frac{\Omega}{2}(B + B^T). \quad (\text{B3})$$

The two-excitation states can still be solved, because the energy equations from Eq. (61) still hold. Therefore, the wave functions are still combinations of four different Choy-Haldane states, just with different weights λ . Since the second equation has one extra term when the interspecies interaction is nonvanishing, the equations determining λ become slightly modified,

$$\sum_{i=1}^4 J_1 \tilde{u}_i \lambda_i (1 + s_i) = U_1 \sum_{i=1}^4 \lambda_i (1 + s_i), \quad (\text{B4})$$

$$\sum_{i=1}^4 J_2 \tilde{u}_i \lambda'_i (1 + s_i) = U_2 \sum_{i=1}^4 \lambda'_i (1 + s_i), \quad (\text{B5})$$

$$\begin{aligned} & \sum_{i=1}^4 \lambda_i (\epsilon - \omega_{k_i} - \omega_{q_i}) [(J_1 + J_2) \tilde{u}_i (1 + s_i) \\ & - (J_1 - J_2) 2i (\sin k_i + \sin q_i) \kappa_i (1 - s_i)] \\ & = 2\Omega U_3 \sum_{i=0}^4 \lambda_i (\epsilon - \omega_{k_i} - \omega_{q_i}) (1 + s_i), \end{aligned} \quad (\text{B6})$$

$$\sum_{i=1}^4 \kappa_i \lambda_i (\epsilon - \omega_{k_i} - \omega_{q_i}) (1 - s_i) = 0. \quad (\text{B7})$$

With these equations, we now discuss a few limits.

(i) When $U_1 = U$, $U_2 = 0$, and $J_1 = J_2 = J$, these equations are simplified and $\lambda'_{1,2} = \lambda_{1,2}$ and $\lambda'_3 = -\lambda_3$. We let $u_i \equiv U_i/J$,

$$\sum_{i=1}^3 \lambda_i (1 + s_i) \tilde{u}_i = u \sum_{i=1}^3 \lambda_i (1 + s_i), \quad (\text{B8})$$

$$\sum_{i=1}^3 \lambda'_i (1 + s_i) \tilde{u}_i = u_2 \sum_{i=1}^3 \lambda'_i (1 + s_i) = 0, \quad (\text{B9})$$

$$\sum_{i=1}^2 (-1)^i \lambda_i (1 + s_i) \tilde{u}_i = u_3 \left(\sum_{i=1}^2 (-1)^i \lambda_i (1 + s_i) \right). \quad (\text{B10})$$

(ii) When $U_1 = U_2 = U$ and $J_1 = J_2 = J$, these equations become

$$\begin{aligned} & \lambda_1 (1 + s_1) \tilde{u}_1 + \lambda_2 (1 + s_2) \tilde{u}_2 \\ & = u [\lambda_1 (1 + s_1) + \lambda_2 (1 + s_2)], \end{aligned} \quad (\text{B11})$$

$$\begin{aligned} & \lambda_1 (1 + s_1) \tilde{u}_1 - \lambda_2 (1 + s_2) \tilde{u}_2 \\ & = u_3 [\lambda_1 (1 + s_1) - \lambda_2 (1 + s_2)], \end{aligned} \quad (\text{B12})$$

$$\tilde{u}_3 = u_3. \quad (\text{B13})$$

It turns out that when $U_3 \neq 0$, there are the same three types of solutions we saw in Sec. VII: (i) $A = -C = HC_0$ and $B = 0$, (ii) $A = C = \lambda_1 HC_1 + \lambda_2 HC_2$, and (iii) $B = -B^T$ and $A = C = 0$. Turning on the interspecies interaction U_3 , the first and third types of states stay the same. For the second type of states, they are still combinations of the same two Choy-Haldane states, except that $\lambda_{1,2}$ are different now. We can further take the case when $U_1 = U_2 = U_3 = U$; then the resulting solutions of the second type are just ($\tilde{u}_1 = u$, $\lambda_2 = 0$) and ($\tilde{u}_2 = u$, $\lambda_1 = 0$). This means that when all the inter- and intraspecies interactions are the same, the two-particle states are simply Choy-Haldane states (and antisymmetric states) $|\psi\rangle = |HC_i\rangle$, whose momenta satisfy energy equations $\epsilon = \omega_k + \omega_q + c$, with $c = 0, \pm 2\Omega$.

-
- [1] M. P. A. Fisher, P. B. Weichman, G. Grinstein, and D. S. Fisher, Boson localization and the superfluid-insulator transition, *Phys. Rev. B* **40**, 546 (1989).
- [2] M. Greiner, O. Mandel, T. Esslinger, T. W. Hänsch, and I. Bloch, Quantum phase transition from a superfluid to a Mott insulator in a gas of ultracold atoms, *Nature (London)* **415**, 39 (2002).
- [3] M. Lewenstein, A. Sanpera, V. Ahufinger, B. Damski, A. Sen(De), and U. Sen, Ultracold atomic gases in optical lattices: Mimicking condensed matter physics and beyond, *Adv. Phys.* **56**, 243 (2007).
- [4] I. Bloch, J. Dalibard, and W. Zwerger, Many-body physics with ultracold gases, *Rev. Mod. Phys.* **80**, 885 (2008).
- [5] C. Gross and I. Bloch, Quantum simulations with ultracold atoms in optical lattices, *Science* **357**, 995 (2017).
- [6] M. Bruderer, A. Klein, S. R. Clark, and D. Jaksch, Polaron physics in optical lattices, *Phys. Rev. A* **76**, 011605(R) (2007).
- [7] B. Gadway, D. Pertot, R. Reimann, and D. Schneble, Superfluidity of Interacting Bosonic Mixtures in Optical Lattices, *Phys. Rev. Lett.* **105**, 045303 (2010).
- [8] A. B. Kuklov and B. V. Svistunov, Counterflow Superfluidity of Two-Species Ultracold Atoms in a Commensurate Optical Lattice, *Phys. Rev. Lett.* **90**, 100401 (2003).
- [9] E. Altman, W. Hofstetter, E. Demler, and M. D. Lukin, Phase diagram of two-component bosons on an optical lattice, *New J. Phys.* **5**, 113 (2003).
- [10] P. N. Jepsen, J. Amato-Grill, I. Dimitrova, W. W. Ho, E. Demler, and W. Ketterle, Spin transport in a tunable Heisenberg model realized with ultracold atoms, *Nature (London)* **588**, 403 (2020).
- [11] W. C. Chung, J. de Hond, J. Xiang, E. Cruz-Colón, and W. Ketterle, Tunable Single-Ion Anisotropy in Spin-1 Models Realized with Ultracold Atoms, *Phys. Rev. Lett.* **126**, 163203 (2021).
- [12] I. de Vega, D. Porras, and J. I. Cirac, Matter-Wave Emission in Optical Lattices: Single Particle and Collective Effects, *Phys. Rev. Lett.* **101**, 260404 (2008).
- [13] C. Navarrete-Benlloch, I. de Vega, D. Porras, and J. I. Cirac, Simulating quantum-optical phenomena with cold atoms in optical lattices, *New J. Phys.* **13**, 023024 (2011).

- [14] M. Stewart, L. Krinner, A. Pazmiño, and D. Schneble, Analysis of non-Markovian coupling of a lattice-trapped atom to free space, *Phys. Rev. A* **95**, 013626 (2017).
- [15] A. Lanuza, J. Kwon, Y. Kim, and D. Schneble, Multiband and array effects in matter-wave-based waveguide QED, *Phys. Rev. A* **105**, 023703 (2022).
- [16] G. Calajó, F. Ciccarello, D. Chang, and P. Rabl, Atom-field dressed states in slow-light waveguide QED, *Phys. Rev. A* **93**, 033833 (2016).
- [17] A. Goban, C.-L. Hung, S.-P. Yu, J. D. Hood, J. A. Muniz, J. H. Lee, M. J. Martin, A. C. McClung, K. S. Choi, D. E. Chang, O. Painter, and H. J. Kimble, Atom–light interactions in photonic crystals, *Nat. Commun.* **5**, 3808 (2014).
- [18] P. Lodahl, S. Mahmoodian, and S. Stobbe, Interfacing single photons and single quantum dots with photonic nanostructures, *Rev. Mod. Phys.* **87**, 347 (2015).
- [19] P. Facchi, D. Lonigro, S. Pascazio, F. V. Pepe, and D. Pomarico, Bound states in the continuum for an array of quantum emitters, *Phys. Rev. A* **100**, 023834 (2019).
- [20] P. Facchi, M. S. Kim, S. Pascazio, F. V. Pepe, D. Pomarico, and T. Tufarelli, Bound states and entanglement generation in waveguide quantum electrodynamics, *Phys. Rev. A* **94**, 043839 (2016).
- [21] S. J. Masson and A. Asenjo-Garcia, Atomic-waveguide quantum electrodynamics, *Phys. Rev. Research* **2**, 043213 (2020).
- [22] E. Sánchez-Burillo, D. Zueco, L. Martín-Moreno, and J. J. García-Ripoll, Dynamical signatures of bound states in waveguide QED, *Phys. Rev. A* **96**, 023831 (2017).
- [23] L. Krinner, M. Stewart, A. Pazmiño, J. Kwon, and D. Schneble, Spontaneous emission of matter waves from a tunable open quantum system, *Nature (London)* **559**, 589 (2018).
- [24] T. Shi, Y.-H. Wu, A. González-Tudela, and J. I. Cirac, Effective many-body Hamiltonians of qubit-photon bound states, *New J. Phys.* **20**, 105005 (2018).
- [25] J. Kwon, Y. Kim, A. Lanuza, and D. Schneble, Formation of matter-wave polaritons in an optical lattice, *Nat. Phys.* (2022), doi: [10.1038/s41567-022-01565-4](https://doi.org/10.1038/s41567-022-01565-4)
- [26] M. J. Hartmann, F. G. S. L. Brandão, and M. B. Plenio, Strongly interacting polaritons in coupled arrays of cavities, *Nat. Phys.* **2**, 849 (2006).
- [27] A. D. Greentree, C. Tahan, J. H. Cole, and L. C. L. Hollenberg, Quantum phase transitions of light, *Nat. Phys.* **2**, 856 (2006).
- [28] O. Astafiev, Jr. A. M. Zagoskin, A. Abdumalikov, Y. A. Pashkin, T. Yamamoto, K. Inomata, Y. Nakamura, and J. S. Tsai, Resonance fluorescence of a single artificial atom, *Science* **327**, 840 (2010).
- [29] I.-C. Hoi, C. M. Wilson, G. Johansson, T. Palomaki, B. Peropadre, and P. Delsing, Demonstration of a Single-Photon Router in the Microwave Regime, *Phys. Rev. Lett.* **107**, 073601 (2011).
- [30] A. F. Van Loo, A. Fedorov, K. Lalumiere, B. C. Sanders, A. Blais, and A. Wallraff, Photon-mediated interactions between distant artificial atoms, *Science* **342**, 1494 (2013).
- [31] J. A. Mlynek, A. A. Abdumalikov, C. Eichler, and A. Wallraff, Observation of Dicke superradiance for two artificial atoms in a cavity with high decay rate, *Nat. Commun.* **5**, 5186 (2014).
- [32] R. Ma, B. Saxberg, C. Owens, N. Leung, Y. Lu, J. Simon, and D. I. Schuster, A dissipatively stabilized Mott insulator of photons, *Nature (London)* **566**, 51 (2019).
- [33] S. John and J. Wang, Quantum Electrodynamics near a Photonic Band Gap: Photon Bound States and Dressed Atoms, *Phys. Rev. Lett.* **64**, 2418 (1990).
- [34] A. L. Chudnovskiy, D. M. Gangardt, and A. Kamenev, Doublon Relaxation in the Bose-Hubbard Model, *Phys. Rev. Lett.* **108**, 085302 (2012).
- [35] K. Winkler, G. Thalhammer, F. Lang, R. Grimm, J. H. Denschlag, A. Daley, A. Kantian, H. Büchler, and P. Zoller, Repulsively bound atom pairs in an optical lattice, *Nature (London)* **441**, 853 (2006).
- [36] C. W. Hsu, B. Zhen, A. D. Stone, J. D. Joannopoulos, and M. Soljačić, Bound states in the continuum, *Nat. Rev. Mater.* **1**, 16048 (2016).
- [37] G. Calajó, Y.-L. L. Fang, H. U. Baranger, and F. Ciccarello, Exciting a Bound State in the Continuum through Multiphoton Scattering Plus Delayed Quantum Feedback, *Phys. Rev. Lett.* **122**, 073601 (2019).
- [38] S. Longhi and G. Della Valle, Tamm-Hubbard surface states in the continuum, *J. Phys.: Condens. Matter* **25**, 235601 (2013).
- [39] J. M. Zhang, D. Braak, and M. Kollar, Bound states in the one-dimensional two-particle Hubbard model with an impurity, *Phys. Rev. A* **87**, 023613 (2013).
- [40] G. Della Valle and S. Longhi, Floquet-Hubbard bound states in the continuum, *Phys. Rev. B* **89**, 115118 (2014).
- [41] H. J. Kimble, The quantum internet, *Nature (London)* **453**, 1023 (2008).
- [42] A. I. Lvovsky, B. C. Sanders, and W. Tittel, Optical quantum memory, *Nat. Photon.* **3**, 706 (2009).
- [43] E. Saglamyurek, T. Hrushevskiy, A. Rastogi, K. Heshami, and L. J. LeBlanc, Coherent storage and manipulation of broadband photons via dynamically controlled Autler–Townes splitting, *Nat. Photon.* **12**, 774 (2018).
- [44] F. H. L. Essler, H. Frahm, F. Göhmann, A. Klümper, and V. E. Korepin, *The One-Dimensional Hubbard Model* (Cambridge University Press, Cambridge, 2005).
- [45] M. Valiente and D. Petrosyan, Two-particle states in the Hubbard model, *J. Phys. B* **41**, 161002 (2008).
- [46] M. Valiente, Lattice two-body problem with arbitrary finite-range interactions, *Phys. Rev. A* **81**, 042102 (2010).
- [47] M. Valiente and D. Petrosyan, Scattering resonances and two-particle bound states of the extended Hubbard model, *J. Phys. B* **42**, 121001 (2009).
- [48] A. A. Stepanenko and M. A. Gorbach, Interaction-induced topological states of photon pairs, *Phys. Rev. A* **102**, 013510 (2020).
- [49] T. Choy, Some exact results for a degenerate Hubbard model in one dimension, *Phys. Lett. A* **80**, 49 (1980).
- [50] T. Choy and F. Haldane, Failure of Bethe-ansatz solutions of generalisations of the Hubbard chain to arbitrary permutation symmetry, *Phys. Lett. A* **90**, 83 (1982).
- [51] N. Oelkers and J. Links, Ground-state properties of the attractive one-dimensional Bose-Hubbard model, *Phys. Rev. B* **75**, 115119 (2007).
- [52] J. M. Zhang, D. Braak, and M. Kollar, Bound States in the Continuum Realized in the One-Dimensional Two-Particle Hubbard Model with an Impurity, *Phys. Rev. Lett.* **109**, 116405 (2012).
- [53] D. Cheng, B. Peng, D.-W. Wang, X. Chen, L. Yuan, and S. Fan, Arbitrary synthetic dimensions via multiboson dynamics on a one-dimensional lattice, *Phys. Rev. Research* **3**, 033069 (2021).

- [54] B. Kramer and A. MacKinnon, Localization: Theory and experiment, *Rep. Prog. Phys.* **56**, 1469 (1993).
- [55] M. McDonald, J. Trisnadi, K.-X. Yao, and C. Chin, Superresolution Microscopy of Cold Atoms in an Optical Lattice, *Phys. Rev. X* **9**, 021001 (2019).
- [56] I. Morera, G. E. Astrakharchik, A. Polls, and B. Juliá-Díaz, Universal Dimerized Quantum Droplets in a One-Dimensional Lattice, *Phys. Rev. Lett.* **126**, 023001 (2021).
- [57] W. S. Bakr, J. I. Gillen, A. Peng, S. Fölling, and M. Greiner, A quantum gas microscope for detecting single atoms in a Hubbard-regime optical lattice, *Nature (London)* **462**, 74 (2009).
- [58] M. S. Blok, V. V. Ramasesh, T. Schuster, K. O'Brien, J. M. Kreikebaum, D. Dahlen, A. Morvan, B. Yoshida, N. Y. Yao, and I. Siddiqi, Quantum Information Scrambling on a Superconducting Qutrit Processor, *Phys. Rev. X* **11**, 021010 (2021).